

# Charm couplings and form factors in QCD sum rules

M.E. Bracco<sup>1</sup>, M. Chiapparini<sup>2</sup>, F.S. Navarra<sup>3</sup>, M. Nielsen<sup>3</sup>

<sup>1</sup>Faculdade de Tecnologia, Universidade do Estado do Rio de Janeiro,  
Rod. Presidente Dutra Km 298, Polo Industrial, 27537-000, Resende, RJ, Brazil

<sup>2</sup>Instituto de Física, Universidade do Estado do Rio de Janeiro,  
Rua São Francisco Xavier 524, 20550-900 Rio de Janeiro, RJ, Brazil

<sup>3</sup>Instituto de Física, Universidade de São Paulo,  
C.P. 66318, 05389-970 São Paulo, SP, Brazil

February 17, 2022

## Abstract

We review the calculations of form factors and coupling constants in vertices with charm mesons in the framework of QCD sum rules. We first discuss the motivation for this work, describing possible applications of these form factors to heavy ion collisions and to B decays. We then present an introduction to the method of QCD sum rules and describe how to work with the three-point function. We give special attention to the procedure employed to extrapolate results obtained in the deep euclidean region to the poles of the particles, located in the time-like region. We present a table of ready-to-use parametrizations of all the form factors, which are relevant for the processes mentioned in the introduction. We discuss the uncertainties in our results. We also give the coupling constants and compare them with estimates obtained with other methods. Finally we apply our results to the calculation of the cross section of the reaction  $J/\psi + \pi \rightarrow D + \bar{D}^*$ .

*Prepared for publication in Prog. Part. Nucl. Phys.*

# Contents

<b>1</b>	<b>Introduction</b>	<b>3</b>
<b>2</b>	<b>QCD Sum Rules</b>	<b>5</b>
2.1	The two-point correlation functions . . . . .	5
2.2	The spectral density . . . . .	6
2.3	The mass sum rule . . . . .	7
2.4	The three-point function . . . . .	8
2.5	The OPE side . . . . .	8
2.6	The phenomenological side . . . . .	9
2.7	The sum rule . . . . .	10
2.8	Effective Lagrangians . . . . .	11
2.9	Couplings . . . . .	13
<b>3</b>	<b>Evaluation of the sum rules</b>	<b>14</b>
3.1	Numerical inputs . . . . .	14
3.2	Borel stability . . . . .	14
3.3	OPE convergence . . . . .	16
3.4	Pole versus continuum . . . . .	17
3.5	Continuum threshold effects . . . . .	18
3.6	Choice of the structure . . . . .	19
<b>4</b>	<b>Form factors</b>	<b>21</b>
4.1	The extrapolation procedure . . . . .	21
4.2	Hadronic loops . . . . .	23
<b>5</b>	<b>Results</b>	<b>26</b>
5.1	Form factors and couplings . . . . .	26
5.2	Uncertainties . . . . .	28
<b>6</b>	<b>Discussion</b>	<b>33</b>
6.1	SU(4) and HQET . . . . .	34
6.2	Light cone sum rules . . . . .	34
6.3	Vector meson dominance . . . . .	35
<b>7</b>	<b><math>J/\psi</math> absorption and production</b>	<b>36</b>
<b>8</b>	<b>Summary</b>	<b>40</b>
	<b>Acknowledgments</b>	<b>41</b>

# 1 Introduction

When we write the high energy electron-proton scattering cross section using the Feynman rules of quantum electrodynamics (QED), we do not know how to write the interaction between the photon and the proton when the latter is an extended and composite object. In order to organize and parametrize our ignorance making use of general principles, such as charge conservation, we introduce functions of the involved kinematical variables, which are called structure functions. After convenient redefinitions these functions become form factors. The final cross sections, written in terms of form factors are then adjusted to data and, in this way, the form factors are measured. In a particular reference frame, their Fourier transform gives the spacial distribution of charged matter in the proton. This procedure gives a nice “picture” of the proton in space and the most accurate description of its “form”. In lower energy experiments, where also the four momentum transfer ( $q^2$ ) is low, it was possible to determine the electromagnetic form factor (and the charge radius) of the nucleon [1].

QED was also applied to deep inelastic electron-proton scattering with the assumption that the proton is composed by pointlike constituent fermions. In this case the structure functions turned into the parton distribution functions and their precise measurement gave reality to quarks and gluons and illuminated a new world within the proton. In higher energies experiments and very large values of  $q^2$  a very different picture of the nucleon emerged, in which it is made of pointlike particles, the quarks. From these observations one may conclude that, when probing the nucleon, nearly on-shell photons ( $q^2 \simeq 0$ ) recognize sizes whereas highly off-shell photons ( $q^2 \ll 0$ ) do not [1]. This statement is supported by the phenomenologically very successful vector meson dominance hypothesis, according to which real photons are with a large probability converted to vector mesons (which are extended objects) and then interact with the nucleon [2]. HERA data on electron-proton reactions can be well understood introducing a “transverse radius of the photon”, parametrized as

$$r_\gamma \simeq \frac{1}{\sqrt{Q^2 + m^2}}, \quad (1)$$

where  $Q^2 = -q^2$  and  $m$  is the mass of the vector meson considered. This empirical formula tells us that for  $Q^2 \rightarrow \infty$  the photon is pointlike and “resolves” the nucleon target, i.e., identifies its pointlike constituents and does not “see” the size of the nucleon. Moreover, this formula indicates that for  $Q^2 \simeq 0$  and for light mesons (like the  $\rho^0$ ) the photon has appreciable transverse radius and therefore also identifies the global nucleon extension. Finally, in the above formula we may have a heavy vector meson ( $J/\psi$  or  $\Upsilon$ ) which will, either real or virtual, resolve the nucleon into pointlike constituents. This feature nicely explains why the  $J/\psi$  photoproduction cross section grows pronouncedly with the (photon-proton) energy whereas the  $\rho$  cross section grows very slowly. In the former case the compact  $J/\psi$  interacts with the small  $x$  gluons in the protons, which have a fastly growing population. In the latter case, the  $\rho$  identifies the global and slowly growing geometrical size of the proton.

After this glorious history as an important tool in the QED machinery, form factors were calculated in other contexts. In particular they were introduced in the development of effective theories to study interactions of charm particles. In this context, an interesting question is: which are the form factors of the charm mesons when probed by light particles such as photons, pions and  $\rho$  mesons? Apart from their intrinsic value as fundamental knowledge about nature, the answer to this question has immediate applications in hadron physics.

Vertices with three mesons where at least two of them carry charm appear in theories of the charm meson interactions. This kind of theory started to become popular in the late nineties [3], during the analysis of the CERN-SPS data on charmonium production in heavy ion collisions. At that time it was believed that  $J/\psi$  suppression was a good signature of quark gluon plasma formation (QGP) [4]. However a careful evaluation of the background was needed, in order to isolate the signal. In this case the background was the charmonium absorption by light mesons within the hadronic fireball

formed at the late stage of these collisions. Since the center of mass energy of these collisions was of the order of magnitude of the temperature, i.e.  $\simeq 100 - 200$  MeV, the interaction regime was clearly non-perturbative and the best tools were the effective Lagrangian models with charm mesons [3, 5]. From these Lagrangians one can derive the Feynman rules and compute scattering amplitudes. In order to avoid infinities one can introduce form factors in the vertices. In phenomenological applications, these form factors contain a parameter  $\Lambda$  which plays the role of a cut-off. In fact, even diagrams which give finite contributions to the cross sections must contain form factors. Otherwise the obtained cross sections are unacceptably large. After the introduction of form factors the results for the charmonium interaction cross section become quite reasonable. However these results depend too strongly on the choice of the cut-off parameter. In QCD sum rules (QCDSR) we can calculate these form factors from first principles, eliminating the freedom in the choice of parameters.

At this point one might argue that this program is futile for at least two reasons. In first place one might say that one can compute cross sections such as, for example,  $J/\psi + \pi \rightarrow D + \bar{D}$ , directly from QCDSR [6] and it is not necessary to compute form factors. This statement is in principle correct. In practice however, the direct calculation of cross sections with QCDSR requires the use of the four-point function, which is much less precise than the three and two-point functions. It is not clear, for example, whether one should perform one, two or even three Borel transforms. In second place one might say that it is more promising to develop a chiral perturbation theory for these interactions, where one eliminates form factors [7]. This may indeed be the case, but for now this kind of theory is in a very preliminary stage. Moreover, in effective theories one needs the coupling constants. In the case of the charm three meson vertices these couplings (with the exception of the  $D^*D\pi$  coupling constant) are not measurable. They can be calculated in QCDSR, as a by-product of the calculation of form factors.

The experimental study of interactions of charmed mesons with nucleons and also with light mesons will be one of the main topics of the scientific program of the PANDA and CBM experiments at the future FAIR facility at GSI [8].

So far we have been emphasizing the usefulness of charm form factors in the calculation of charmonium interaction cross sections. However, this is just one of the several applications of these form factors. Another context where they are needed is in heavy meson decays. Since 2003, due to the precise measurements of  $B$  decays performed by BELLE, BES and BABAR, charm form factors gained a new relevance. In  $B$  decays new particles have been observed, such as the  $D_{sJ}(2317)$  and the  $X(3872)$  [9, 10]. These particles decay very often into an intermediate two body state, which then undergoes final state interactions, with the exchange of one or more virtual mesons [11]. As an example of specific situation we may consider the decay  $X(3872) \rightarrow J/\psi + \rho$ . This decay may proceed in two steps. First the  $X$  decays into a  $D - D^*$  intermediate state and then these two particles exchange a  $D^*$  producing the final  $J/\psi$  and  $\rho$  [12]. This process is illustrated in Fig. 1. In order to compute the effect of these interactions in the final decay rate we need the  $\rho D^* D^*$  and  $J/\psi D^* D$  form factors.

Besides the decays, charm form factors may be needed to understand the structure of these newly observed charm states. In [13, 14, 15] it has been suggested that some of these states are dynamically generated resonances from the vector-vector mesonic interaction. Here we have box diagrams with virtual meson exchanges and vertices which need form factors.

In this article we review our works on charm form factors [16, 17, 18, 19, 20, 21, 22, 23, 24] calculated with QCD sum rules [9, 25, 26, 27]. In doing so we compare our method with other approaches, pointing out their virtues and shortcomings. The text is organized as follows. In Section 2 we present a brief introduction to the QCDSR method, where we emphasise the main concepts and the strategies employed to calculate masses, decay constants, form factors and coupling constants. This introduction is intentionally abstract and “clean”. The subsequent Section 3 illustrates how to calculate numerically all desired quantities. This is where the limitations of the method become clear and also where we show how to circumvent them. In this section we discuss the quality of numerical results and establish certain conditions which must be fulfilled by reliable sum rules. After having defined the method and

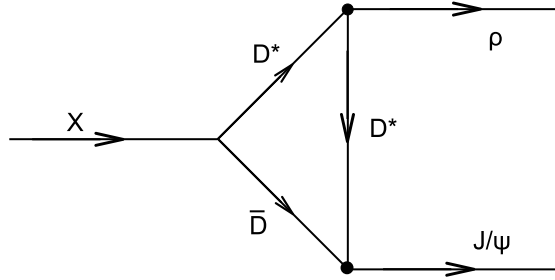


Figure 1: Final state interactions with charm meson loops.

the quality criteria, in Section 4 we present a sample of results obtained for the form factors. We give special attention to one particular form factor and the respective vertex coupling constant:  $D^*D\pi$ . This vertex is special because is the only one directly accessible to experiments. Its coupling constant was measured and several calculations were performed, one of them with lattice QCD techniques. The  $D^*D\pi$  vertex provides the precision test for the different ways of computing the coupling constant. A careful analysis of this vertex resulted in the formulation of a complementary technique (the evaluation of meson loops in the vertex) used to improve the quality of the QCDSR calculations. In Section 5 we show the full compilation of all the already obtained charm form factors, with the corresponding parametrizations, which are ready to be easily employed in phenomenological analyses of vertices with charm mesons. We also present a quantitative study of the uncertainties in our results. In Section 6 we perform a comparison with the results obtained with other approaches. In Section 7 we show an application of the charm form factors to the study of  $J/\psi$  production and absorption by light mesons. Finally, in Section 8 we present a summary of our results.

## 2 QCD Sum Rules

QCD sum rules have been discussed in many reviews [9, 25, 26, 27] emphasizing various aspects of the method. QCDSR are a powerful tool to extract qualitative and quantitative information about hadron properties. In this approach we start with a correlation function that is constructed in terms of hadronic currents, which are chosen so as to have the quantum numbers of the hadrons in question. The basic idea of the formalism is to approach the bound state problem in QCD from short distances and move to larger distances, including non-perturbative effects and using some approximate procedure to extract hadronic masses and couplings. Although we are mostly concerned with the three-point correlation function, sometimes we also need two-point correlation functions. For this reason and also in order to illustrate some basic procedures in QCDSR we devote the next subsections to the discussion of two-point correlators.

### 2.1 The two-point correlation functions

A generic two-point correlation function is usually written as:

$$\Pi(q) \equiv i \int d^4x e^{iq \cdot x} \langle 0 | T[j(x)j^\dagger(0)] | 0 \rangle , \quad (2)$$

where  $j(x)$  is a current with the quantum numbers of the hadron which we want to study.

In QCDSR we assume that the correlation functions may be written at both the quark and the hadron levels. Identifying the hadronic representation with the corresponding representation in terms of quarks and gluons, we obtain the sum rule, from which we can determine hadron properties. In the QCD side we proceed with the calculation of the correlation function using the operator product expansion (OPE), which is formulated with Wilson coefficients and local operators in terms of the non-perturbative structure of the QCD vacuum. In order to apply this method to the correlation function (2), we have to expand the product of two currents in a series of local operators:

$$\Pi^{OPE}(q^2) = i \int d^4x e^{iq \cdot x} \langle 0 | T[j(x)j^\dagger(0)] | 0 \rangle = \sum_n C_n(q^2) \langle 0 | \hat{O}_n | 0 \rangle, \quad (3)$$

where the set  $\{\hat{O}_n\}$  includes all local gauge invariant operators expressible in terms of light quark and gluon fields. By construction the coefficients  $C_n(Q^2)$  ( $Q^2 = -q^2$ ) in Eq. (3) include only short-distance effects. Therefore, they can be evaluated perturbatively. Non-perturbative long-distance effects are contained only in the local operators. In the OPE expansion, the operators are ordered according to their dimension  $n$ . The lowest-dimension operator with  $n = 0$  is the unit operator associated with the perturbative contribution:  $C_0(Q^2) = \Pi^{per}(Q^2)$ ,  $\hat{O}_0 = 1$ . The QCD vacuum fields are represented in (3) in the form of the so called vacuum condensates. The lowest dimension condensates are the quark condensate of dimension three:  $\langle 0 | \hat{O}_3 | 0 \rangle = \langle \bar{q}q \rangle$ , and the gluon condensate of dimension four:  $\langle 0 | \hat{O}_4 | 0 \rangle = \langle g^2 G^2 \rangle$ . The contributions of higher dimension condensates are suppressed by large powers of  $\Lambda_{QCD}^2/Q^2$ , where  $\Lambda_{QCD}$  is the typical long-distance scale. Therefore, even at intermediate  $Q^2 \sim 1 \text{ GeV}^2$ , the expansion in Eq. (3) can be safely truncated after a few terms.

## 2.2 The spectral density

The hadronic (or “phenomenological”) representation of the correlation function in Eq. (2) can be written as a dispersion relation:

$$\Pi^{phen}(q^2) = - \int ds \frac{\rho(s)}{q^2 - s + i\epsilon} + \dots, \quad (4)$$

The dots in the above equation represent subtraction terms. The spectral density is given by the imaginary part of the correlation function:

$$\rho(s) = \frac{1}{\pi} \text{Im}[\Pi(s)]. \quad (5)$$

The evaluation of  $\rho(s)$  is simpler than the evaluation of the correlation function itself, and the knowledge of  $\rho(s)$  allows one to recover the whole function  $\Pi(q^2)$  through the integral in Eq. (4).

The current  $j$  ( $j^\dagger$ ) appearing in (2) and (3) is an operator that annihilates (creates) all hadronic states that have the same quantum numbers as  $j$ . Consequently,  $\Pi(q^2)$  contains information not only about the low mass hadron of interest, but also about all excited states with the same quantum numbers. When comparing a set of hadrons with the same quantum numbers, the lowest resonance is often fairly narrow, whereas higher mass states are broader. We can therefore parametrize the spectral density as a single sharp pole, representing the lowest resonance of mass  $m$ , plus a smooth continuum, representing higher mass states:

$$\rho(s) = \lambda^2 \delta(s - m^2) + \rho^{cont}(s), \quad (6)$$

In the above Equation the parameter  $\lambda$  represents the coupling of the current to the low mass hadron  $H$ :

$$\langle 0 | j | H \rangle = \lambda. \quad (7)$$

For simplicity, we often assume that the continuum contribution to the spectral density,  $\rho^{cont}(s)$  in Eq. (6), vanishes below a certain continuum threshold  $s_0$ . In order to keep the number of parameters as small as possible, we assume that above  $s_0$  the spectral density is given by the result obtained with the OPE. This idea is implemented by the Ansatz proposed in [28]:

$$\rho^{cont}(s) = \rho^{OPE}(s)\Theta(s - s_0). \quad (8)$$

This is called quark-hadron duality.

## 2.3 The mass sum rule

The sum rule is obtained from the matching of the two descriptions of the correlator:

$$\Pi^{phen}(Q^2) = \Pi^{OPE}(Q^2). \quad (9)$$

However, such a matching is not yet practical. The phenomenological description is significantly dominated by the lowest pole only for sufficiently small  $Q^2$ , or even better, timelike  $q^2$  near the pole. On the other hand, the OPE side is only valid at a sufficiently large spacelike  $Q^2$ . In order to improve the overlap between the two sides of the sum rule, we apply the Borel transform:

$$\mathcal{B}_{M^2}[\Pi(q^2)] = \lim_{\substack{-q^2, n \rightarrow \infty \\ -q^2/n = M^2}} \frac{(-q^2)^{n+1}}{n!} \left( \frac{d}{dq^2} \right)^n \Pi(q^2). \quad (10)$$

It is interesting to notice that:

$$\mathcal{B}_{M^2} [q^{2n}] = 0, \quad n > 0. \quad (11)$$

This means that all the subtractions terms in Eq. (4) are eliminated by the Borel transform. Another important feature of the Borel transform is the fact that:

$$\mathcal{B}_{M^2} \left[ \frac{1}{(m^2 - q^2)^n} \right] = \frac{1}{(n-1)!} \frac{e^{-m^2/M^2}}{(M^2)^{n-1}}, \quad n > 0. \quad (12)$$

Therefore, the Borel transform exponentially suppresses the contribution from excited resonances and continuum states in the phenomenological side. In the OPE side the Borel transform suppresses the contribution from higher dimension condensates by a factorial term, improving the OPE convergence. After making a Borel transform on both sides of the sum rule, and transferring the continuum contribution to the OPE side, the sum rule can be written as

$$\lambda^2 e^{-m^2/M^2} = \int_{s_{min}}^{s_0} ds e^{-s/M^2} \rho^{OPE}(s). \quad (13)$$

The mass of the low-lying state,  $m$ , can be determined by taking the derivative of Eq. (13) with respect to  $1/M^2$ , and dividing the result by Eq. (13). This gives:

$$m^2 = \frac{\int_{s_{min}}^{s_0} ds e^{-s/M^2} s \rho^{OPE}(s)}{\int_{s_{min}}^{s_0} ds e^{-s/M^2} \rho^{OPE}(s)}. \quad (14)$$

Since in the evaluation of both sides of the sum rule we have to make approximations, the value extracted from Eq. (13) will be a function of  $M^2$ . The Borel window is defined as the range of values of  $M^2$  where the two sides of the sum rule have a good overlap and, therefore, information on the lowest resonance can be extracted. In general the Borel window is determined by imposing two different criteria: the minimum value of the Borel mass is fixed by requiring the convergence of the OPE and the maximum value of the Borel mass is determined by imposing the condition that the pole contribution must be bigger than the continuum contribution [29].

## 2.4 The three-point function

The three-point function associated with a generic vertex of three mesons  $M_1$ ,  $M_2$  and  $M_3$  is given by

$$\Gamma(p, p') = \int d^4x d^4y e^{ip' \cdot x} e^{-i(p' - p) \cdot y} \langle 0 | T \{ j_3(x) j_2^\dagger(y) j_1^\dagger(0) \} | 0 \rangle, \quad (15)$$

where the current  $j_i$  represents states with the quantum numbers of the meson  $i$ . As in the previous Section, the correlation function is evaluated in two ways. In the first one, we consider that the currents are composed by quarks and write them in terms of their flavor and color content with the correct quantum numbers. This is the QCD description of the correlator and it gives rise to the QCD side (or OPE side) of the sum rule. In the second way, we write the correlation function in terms of matrix elements of hadronic states which can be extracted from experiment, or calculated with lattice QCD or estimated with effective Lagrangians. In this last approach we never talk about quarks and use all the available experimental information concerning the masses and decay properties of the relevant mesons. This is the hadronic description of the correlator and is called the phenomenological side of the sum rule. After studying both sides separately, we identify one description with the other and write the sum rule.

## 2.5 The OPE side

We start with the current, which has the general form:

$$j_i = \bar{q} \Lambda q, \quad (16)$$

with  $\Lambda = 1, \gamma_\mu, \gamma_5, \gamma_\mu \gamma_5$  for a scalar, vector, pseudo-scalar and axial-vector meson, respectively.  $q$  is the quark spinor field. Since the currents may carry Lorentz indices, so will the vertex function  $\Gamma$ . When we insert the three currents into Eq. (15) we get the vacuum expectation value of the  $T$  product of six quark fields multiplied by Dirac matrices in different points. In this expression we apply Wick's theorem obtaining a series of terms, each of which being the product of contractions (propagators) times a vacuum expectation value of normal ordered operators taken in the QCD vacuum. These latter, in the local approximation, are the QCD condensates. This series is precisely (3) and its first terms are diagrammatically depicted in Fig. 2. The first and leading one is the perturbative term in Fig. 2a. Figs. 2b and 2c show examples of terms with the quark condensate and with the gluon condensate respectively.

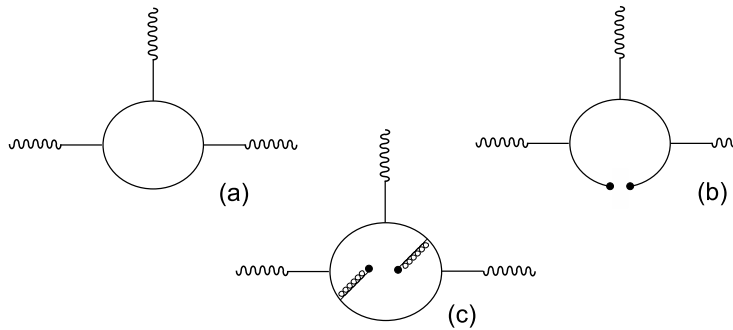


Figure 2: Diagrammatic representation of the first terms of the OPE series for a three-point function. (a) The perturbative term. (b) The quark condensate. (c) The gluon condensate.

The evaluation of (15) in lowest order leads to a loop diagram with three quark propagators. The first corrections to the simple bubble (called the perturbative contribution) come from diagrams where



a quark line “dives” into the vacuum and emerges from it. This contribution to the correlators appears multiplied by the quark condensate  $\langle \bar{q}q \rangle$ . Higher order corrections represent the interactions of the quark lines exchanging gluons among themselves ( $\alpha_s$  corrections) and with the vacuum (gluon condensates and quark-gluon mixed condensates). An equivalent description is obtained performing first the contractions in (15), obtaining three quark propagators and then performing an operator product expansion (OPE) of these propagators. For our purposes it is enough to consider only the first few terms of this expansion:

$$\begin{aligned} S_{ab}(x) &= \langle 0 | T[q_a(x) \bar{q}_b(0)] | 0 \rangle = \frac{i\delta_{ab}}{2\pi^2 x^4} \not{x} - \frac{m_q \delta_{ab}}{4\pi^2 x^2} - \frac{\delta_{ab}}{12} \langle \bar{q}q \rangle + \frac{i\delta_{ab}}{48} m_q \langle \bar{q}q \rangle \not{x} \\ &- \frac{i}{32\pi^2 x^2} T_{ab}^A g_s G_{\mu\nu}^A (\not{x} \sigma^{\mu\nu} + \sigma^{\mu\nu} \not{x}) - \frac{m_q}{32\pi^2} T_{ab}^A g_s G_{\mu\nu}^A \sigma^{\mu\nu} \ln(-x^2). \end{aligned} \quad (17)$$

In the above expression  $x$  is the four-vector which defines the separation between the two quark fields,  $m_q$  is the quark mass,  $T_{ab}^A$  are the SU(3) generators,  $G_{\mu\nu}^A$  is the gluon field tensor and  $\sigma^{\mu\nu}$  is the anticommutator of the Dirac matrices. In (17) the first two terms are related to Fig. 2a, the next two terms are related to Fig. 2b and the last two are related to Fig. 2c. After the contractions and the OPE expansion we arrive at an expression for  $\Gamma$  which has the generic form:

$$\Gamma_{OPE} = \sum_j F_j^{OPE}(p^2, p'^2, q^2) L_j, \quad (18)$$

where  $F_j^{OPE}(p^2, p'^2, q^2)$  are invariant functions of the momenta and  $L_j$  are the structures, i.e., products of Dirac matrices, the metric tensor and the four momenta, carrying Lorentz indices. For each one of the invariant amplitudes appearing in Eq.(18), we can write a double dispersion relation over the virtualities  $p^2$  and  $p'^2$ :

$$F_i^{OPE} = -\frac{1}{4\pi^2} \int_{s_{min}}^{\infty} ds \int_{u_{min}}^{\infty} du \frac{\rho_i^{OPE}(s, u, q^2)}{(s - p^2)(u - p'^2)}, \quad (19)$$

where  $\rho_i^{OPE}(s, u, q^2)$  is the double discontinuity of the amplitude  $F_i^{OPE}(p^2, p'^2, q^2)$  and can be calculated using the Cutkosky's rules. We can work with any structure appearing in Eq.(18), but we must choose those which have less ambiguities in the QCD sum rules approach, which means among other things, a weak influence from the higher dimension condensates. The invariant amplitudes and thus the double discontinuities  $\rho$ , receive contributions from all terms in the OPE. The first one (and dominating) of these contributions must come from the perturbative term.

## 2.6 The phenomenological side

For the phenomenological side we formally repeat the steps mentioned above and find that, as before, the correlation function can be written as a sum of contributions with different tensor structures, i.e. :

$$\Gamma_{phen} = \sum_j F_j^{phen}(p^2, p'^2, q^2) L_j, \quad (20)$$

where  $F_j^{phen}(p^2, p'^2, q^2)$  are invariant functions of the momenta and  $L_j$  are the structures. For each one of the invariant amplitudes appearing in Eq.(20), we can write a double dispersion relation over the virtualities  $p^2$  and  $p'^2$ , holding  $Q^2 = -q^2$  fixed:

$$F_i^{phen} = -\frac{1}{4\pi^2} \int_{s_{min}}^{\infty} ds \int_{u_{min}}^{\infty} du \frac{\rho_i^{phen}(s, u, Q^2)}{(s - p^2)(u - p'^2)}, \quad (21)$$

where  $\rho_i^{phen}(s, u, Q^2)$  is the double discontinuity of the amplitude  $F_i^{phen}(p^2, p'^2, Q^2)$ . The function  $\rho$  can be generically written as:

$$\begin{aligned} \rho_i^{phen}(s, u, Q^2) &= a \delta(s - m_1^2) \delta(u - m_2^2) + b \delta(s - m_1^2) \theta(u - u_0) + \\ &c \delta(u - m_2^2) \theta(s - s_0) + \rho_i^{cont}(s, u, Q^2) \theta(s - s_0) \theta(u - u_0), \end{aligned} \quad (22)$$

where  $s_0$  and  $u_0$  are the continuum threshold parameters. In the above equation the first term represents a kinematical situation where the mesons  $M_1$  and  $M_2$  (with masses  $m_1$  and  $m_2$  respectively) are in the ground state and  $M_3$  is off-shell, having an arbitrary Euclidean four momentum squared  $Q^2$ . The second term represents a situation where the meson  $M_1$  is on-shell but the groundstate of the meson  $M_2$  is absent in the vertex, which contains only its excitations starting at  $u_0$ . The third term represents the inverse situation, where  $M_2$  is on-shell and it is accompanied in the vertex by the excitations of  $M_1$  starting at  $s_0$ . Finally, the last term represents the excitations of  $M_1$  and  $M_2$ , which start at  $s_0$  and  $u_0$  respectively. After a double Borel transform in the variables  $p^2$  and  $p'^2$  the second and third terms are exponentially suppressed. One can then safely assume quark-hadron duality and parametrize the continuum by the double discontinuity of the theoretical part:  $\rho_i^{cont}(s, u, Q^2) = \rho_i^{OPE}(s, u, Q^2)$ . This point is thoughtfully discussed in [30]. Inserting the above expression into (21) (and neglecting the suppressed terms) we have:

$$F_i^{phen} = \Lambda_i^{phen} - \frac{1}{4\pi^2} \int_{s_0}^{\infty} ds \int_{u_0}^{\infty} du \frac{\rho_i^{OPE}(s, u, Q^2)}{(s - p^2)(u - p'^2)}, \quad (23)$$

where  $\Lambda_i^{phen}$  refers to the ground state (or pole) contribution in the structure  $i$ . In order to calculate  $\Lambda_i^{phen}$  we go back to (15) and insert complete sets of hadronic states. After some algebra [31] we obtain:

$$\Lambda_i^{phen} = \frac{f_{M_1} f_{M_2} f_{M_3} \langle M_1 M_2 M_3 \rangle_i}{(p^2 - m_1^2)(p'^2 - m_2^2)(q^2 - m_3^2)}. \quad (24)$$

The meson decay constants appearing in the above equation are defined by the following matrix elements:

$$\langle 0 | j_\mu^V | V \rangle = m_V f_V \epsilon_\mu, \quad (25)$$

$$\langle 0 | j_\mu^A | A \rangle = m_A f_A \epsilon_\mu, \quad (26)$$

$$\langle 0 | j_5 | P \rangle = \frac{m_P^2}{m_q} f_P, \quad (27)$$

and

$$\langle 0 | j_A^\mu | P \rangle = i f_P p^\mu, \quad (28)$$

for vector, axial, pseudoscalar and axial currents respectively. In the above expressions  $\epsilon^\mu$  and  $p^\mu$  are the relevant polarization vector and four momentum of the involved mesons respectively. Eq. (28) refers to the case where a pseudoscalar meson is represented by an axial current, and  $m_q$  in Eq. (27) is the heaviest quark in the pseudoscalar meson  $P$ .

Since the higher states have been considered in the second term of (23), the amplitude  $\langle M_1 M_2 M_3 \rangle$  appearing in (24) refers only to the ground states of the mesons  $M_1$ ,  $M_2$  and  $M_3$  and can be calculated with the help of an effective Lagrangian of the type:

$$\mathcal{L}_{M_1 M_2 M_3} = g_{M_1 M_2 M_3} (\eta \Delta M_1 \Delta M_2 M_3 + hc), \quad (29)$$

where  $\eta = i$  or  $\varepsilon_{\mu\nu\alpha\beta}$ ,  $\Delta = 1$  or  $\partial_\mu$ ,  $hc$  stands for Hermitian conjugates and  $g_{M_1 M_2 M_3}$  is the coupling constant. The choices implied in  $\eta$  and  $\Delta$  depend on the specific combination of mesons.

## 2.7 The sum rule

The sum rule is obtained from the identity:

$$F_i^{phen}(p, p', q) = F_i^{OPE}(p, p', q), \quad (30)$$

that gives

$$\frac{f_{M_1} f_{M_2} f_{M_3} \langle M_1 M_2 M_3 \rangle_i}{(p^2 - m_1^2)(p'^2 - m_2^2)(q^2 - m_3^2)} = -\frac{1}{4\pi^2} \int_{s_{min}}^{s_0} ds \int_{u_{min}}^{u_0} du \frac{\rho_i^{OPE}(s, u, Q^2)}{(s - p^2)(u - p'^2)}, \quad (31)$$

where we have used (19), (23) and (24) and have transferred the dispersion integral in the phenomenological side to the OPE side. Notice that the integration limits are now finite. In order to improve the matching between the two sides of the sum rule and also to suppress the pole-continuum transitions [30] we perform a double Borel transform (10) in the variables  $P^2 = -p^2 \rightarrow M^2$  and  $P'^2 = -p'^2 \rightarrow M'^2$ , on both sides:

$$\frac{f_{M_1} f_{M_2} f_{M_3} \langle M_1 M_2 M_3 \rangle_i}{(Q^2 + m_3^2)} e^{-m_1^2/M^2} e^{-m_2^2/M'^2} = \frac{1}{4\pi^2} \int_{s_{min}}^{s_0} ds \int_{u_{min}}^{u_0} du \rho_i^{OPE}(s, u, Q^2) e^{-s/M^2} e^{-u/M'^2}, \quad (32)$$

From (29) it is clear that the above equation can be solved for the coupling  $g_{M_1 M_2 M_3}$ . Since the squared momenta of the mesons  $M_1$  and  $M_2$  ( $p^2$  and  $p'^2$  respectively) have been replaced by the Borel masses  $M^2$  and  $M'^2$  and then fixed, the coupling  $g$  will be a function only of the remaining Euclidean momentum  $Q^2$ , i.e.,  $g_{M_1 M_2 M_3}^{(M_3)} = g_{M_1 M_2 M_3}^{(M_3)}(Q^2)$  and this is what we call a form factor. The superscripts in parenthesis indicate the meson  $M_3$  is off-shell. At the point  $Q^2 = -m_3^2$  the meson  $M_3$  is on-shell and the form factor becomes the coupling constant. Of course one can not use  $Q^2 = -m_3^2$  in Eq. (32) since the sum rule is only valid for  $Q^2 > 0$ . Therefore, to obtain the coupling constant we will need to use some extrapolation procedure, that will be discussed in Sec. 4.1.

## 2.8 Effective Lagrangians

Since the pioneering work of Matynian and Müller [3], there has been an intense discussion concerning the details and properties of the effective Lagrangians which describe the interactions among charm mesons. Here we follow Refs. [32, 33]. We write down the SU(4) chiral Lagrangian in terms of the mesonic fields:

$$\mathcal{L}_0 = \text{Tr}(\partial_\mu P^\dagger \partial^\mu P) - \frac{1}{2} \text{Tr}(F_{\mu\nu}^\dagger F^{\mu\nu}), \quad (33)$$

where  $F_{\mu\nu} = \partial_\mu V_\nu - \partial_\nu V_\mu$ , and  $P$  and  $V$  denote respectively the properly normalized  $4 \times 4$  pseudoscalar and vector mesons matrices in SU(4) given by:

$$P = \frac{1}{\sqrt{2}} \begin{pmatrix} \frac{\pi^0}{\sqrt{2}} + \frac{\eta}{\sqrt{6}} + \frac{\eta_c}{\sqrt{12}} & \pi^+ & K^+ & \bar{D}^0 \\ \pi^- & -\frac{\pi^0}{\sqrt{2}} + \frac{\eta}{\sqrt{6}} + \frac{\eta_c}{\sqrt{12}} & K^0 & D^- \\ K^- & \bar{K}^0 & -\sqrt{\frac{2}{3}}\eta + \frac{\eta_c}{\sqrt{12}} & D_s^- \\ D^0 & D^+ & D_s^+ & -\frac{3\eta_c}{\sqrt{12}} \end{pmatrix}, \quad (34)$$

$$V = \frac{1}{\sqrt{2}} \begin{pmatrix} \frac{\rho^0}{\sqrt{2}} + \frac{\omega'}{\sqrt{6}} + \frac{J/\psi}{\sqrt{12}} & \rho^+ & K^{*+} & \bar{D}^{*0} \\ \rho^- & -\frac{\rho^0}{\sqrt{2}} + \frac{\omega'}{\sqrt{6}} + \frac{J/\psi}{\sqrt{12}} & K^{*0} & D^{*-} \\ K^{*-} & \bar{K}^{*0} & -\sqrt{\frac{2}{3}}\omega' + \frac{J/\psi}{\sqrt{12}} & D_s^{*-} \\ D^{*0} & D^{*+} & D_s^{*+} & -\frac{3J/\psi}{\sqrt{12}} \end{pmatrix}. \quad (35)$$

In order to obtain the interaction Lagrangian we introduce the following minimal substitutions:

$$\partial_\mu P \rightarrow \partial_\mu P - \frac{ig}{2} [V_\mu, P] \quad (36)$$

$$F_{\mu\nu} \rightarrow \partial_\mu V_\nu - \partial_\nu V_\mu - \frac{ig}{2} [V_\mu, V_\nu]. \quad (37)$$

After using the Hermiticity of  $P$  and  $V$  the resulting Lagrangian reduces to:

$$\begin{aligned}\mathcal{L} = & \mathcal{L}_0 + ig\text{Tr}(\partial^\mu P[P, V_\mu]) - \frac{g^2}{4}\text{Tr}([P, V_\mu]^2) \\ & + ig\text{Tr}(\partial^\mu V^\nu[V_\mu, V_\nu]) + \frac{g^2}{8}\text{Tr}([V_\mu, V_\nu]^2).\end{aligned}\quad (38)$$

The above Lagrangian accounts for vertices of the form  $PPV$  and  $VVV$ , where  $P$  and  $V$  denote pseudoscalar and vector mesons respectively. In order to include the vertices of the form  $PVV$ , it is necessary to use the following anomalous three-particle Lagrangian [33]:

$$\mathcal{L}_{int}^a = -\frac{g_a^2 N_c}{16\pi^2 F_\pi} \epsilon^{\mu\nu\alpha\beta} \text{Tr}(\partial_\mu V_\nu \partial_\alpha V_\beta P). \quad (39)$$

Equations (38) and (39) are used to write the relevant meson effective Lagrangians. For example, in the  $PPV$  ( $VVV$ ) case, we choose two (none) mesons in (34) and one (three) meson in (35) and set all the other elements of these matrices to zero. We then substitute the resulting Equations (34) and (35) into (38) and obtain the interaction Lagrangian for one specific three meson interaction vertex. The coupling constants appearing in these Lagrangians are charge specific (for example:  $g_{D^+D^-J/\psi}$ ) and are functions of the universal  $SU(4)$  couplings  $g$  and  $g_a$ , being thus connected to each other. They are listed in Table 1 and their connection with  $g$  and  $g_a$  is shown. Using a compact notation, the relevant Lagrangians are:

$$\mathcal{L}_{\pi D^* D} = ig_{\pi D^* D} D_\mu^* (\bar{D} \partial^\mu \pi - \partial^\mu \bar{D} \pi), \quad (40)$$

$$\mathcal{L}_{\psi D^* D} = g_{\psi D^* D} \epsilon^{\mu\nu\alpha\beta} \partial_\mu \psi_\nu (\partial_\alpha D_\beta^* \bar{D} + D \partial_\alpha \bar{D}^*{}_\beta), \quad (41)$$

$$\mathcal{L}_{\psi DD} = ig_{\psi DD} \psi^\mu (\partial_\mu D \bar{D} - D \partial_\mu \bar{D}), \quad (42)$$

$$\mathcal{L}_{\pi D^* D^*} = -g_{\pi D^* D^*} \epsilon^{\mu\nu\alpha\beta} \partial_\mu D_\nu^* \pi \partial_\alpha \bar{D}^*{}_\beta, \quad (43)$$

$$\begin{aligned}\mathcal{L}_{\psi D^* D^*} = & ig_{\psi D^* D^*} \left[ \psi^\mu (\partial_\mu D^{*\nu} \bar{D}_\nu^* - D^{*\nu} \partial_\mu \bar{D}_\nu^*) \right. \\ & \left. + (\partial_\mu \psi_\nu D^{*\nu} - \psi_\nu \partial_\mu D_\nu^*) \bar{D}^{*\mu} + D^{*\mu} (\psi^\nu \partial_\mu \bar{D}_\nu^* - \partial_\mu \psi_\nu \bar{D}^{*\nu}) \right],\end{aligned}\quad (44)$$

$$\mathcal{L}_{\rho DD} = -ig_{\rho DD} \rho^\mu (\partial_\mu D \bar{D} - D \partial_\mu \bar{D}), \quad (45)$$

$$\begin{aligned}\mathcal{L}_{\rho D^* D^*} = & ig_{\rho D^* D^*} \left[ \rho^\mu (\partial_\mu D^{*\nu} \bar{D}_\nu^* - D^{*\nu} \partial_\mu \bar{D}_\nu^*) \right. \\ & \left. + (\partial_\mu \rho_\nu D^{*\nu} - \rho_\nu \partial_\mu D_\nu^*) \bar{D}^{*\mu} + D^{*\mu} (\rho^\nu \partial_\mu \bar{D}_\nu^* - \partial_\mu \rho_\nu \bar{D}^{*\nu}) \right],\end{aligned}\quad (46)$$

$$\mathcal{L}_{\rho D^* D} = g_{\rho D^* D} \epsilon^{\mu\nu\alpha\beta} \partial_\mu \rho_\nu (\partial_\alpha D_\beta^* \bar{D} + D \partial_\alpha \bar{D}^*{}_\beta) \quad (47)$$

For future applications we present below the following Lagrangians containing quartic vertices:

$$\mathcal{L}_{\psi DD\pi} = ig_{\psi DD\pi} \epsilon^{\mu\nu\alpha\beta} \psi_\mu \partial_\nu D \partial_\alpha \pi \partial_\beta \bar{D}, \quad (48)$$

$$\mathcal{L}_{\psi D^* D\pi} = -g_{\psi D^* D\pi} \psi^\mu (D \pi \bar{D}_\mu^* + D_\mu^* \pi \bar{D}), \quad (49)$$

$$\mathcal{L}_{\psi D^* D^* \pi} = ig_{\psi D^* D^* \pi} \epsilon^{\mu\nu\alpha\beta} \psi_\mu D_\nu^* \partial_\alpha \pi \bar{D}^*{}_\beta + ih_{\psi D^* D^* \pi} \epsilon^{\mu\nu\alpha\beta} \partial_\mu \psi_\nu D_\alpha^* \pi \bar{D}^*{}_\beta, \quad (50)$$

where it is understood that, when doing practical calculations, charges must be specified in the above expressions. As it will be seen in the next section, after having calculated all specific coupling constants, we can, using some appropriate convention, write them all in terms of generic coupling constants  $g_{M_1 M_2 M_3}$ .

From the above Lagrangians we can derive the Feynman rule for the vertex (the amplitude  $\langle M_1 M_2 M_3 \rangle$ ) which, as it can be seen, depends on the relevant polarization vector, momenta and on the coupling

$g_{M_1 M_2 M_3}$ . The latter is the unknown, which will be determined by solving the sum rule. For example, for the  $D^* D \pi$  vertex we get:

$$\langle D^*(p) | \pi(q) D(p-q) \rangle = g_{D^* D \pi}(q^2) q_\mu \varepsilon^\mu(p), \quad (51)$$

where the momentum assignment is specified in the brackets and  $\varepsilon^\mu$  is the polarization vector of the  $D^*$ .

## 2.9 Couplings

Coupling	Normal Vertices
$g/(4\sqrt{3})$	$\omega D^0 \bar{D}^0, \omega D^+ D^-, \omega D^{*0} \bar{D}^{*0}, \omega D^{*+} \bar{D}^{*-}$ $\eta D^{*0} \bar{D}^{*0}, \eta D^\pm D^{*\mp}$
$g/4$	$\pi^0 D^0 \bar{D}^0, \pi^0 D^\pm D^{*\mp}$ $\rho^0 D^0 \bar{D}^0, \rho^0 D^+ D^-, \rho^0 D^{*0} \bar{D}^{*0}, \rho^0 D^{*+} \bar{D}^{*-}$
$g/(2\sqrt{2})$	$\pi^+ D^0 \bar{D}^{*-}, \pi^- \bar{D}^0 D^{*+}, \pi^+ D^- \bar{D}^{*0}, \pi^- D^+ D^{*0}$ $\rho^+ D^0 \bar{D}^-, \rho^- \bar{D}^0 D^+, \rho^+ D^{*0} \bar{D}^{*-}, \rho^- \bar{D}^{*0} D^{*+}$
$g/\sqrt{6}$	$\eta_c D^0 \bar{D}^0, \eta_c D^\pm D^{*\mp}$ $J/\psi D^0 \bar{D}^0, J/\psi D^+ D^-, J/\psi D^{*0} \bar{D}^{*0}, J/\psi D^{*\pm} \bar{D}^{*\mp}$
Anomalous Vertices	
$\alpha/(4\sqrt{6})$	$\eta_c \rho^0 \rho^0, \eta_c \rho^+ \rho^-, \eta_c \omega \omega$ $J/\psi \pi^0 \rho^0, J/\psi \pi^\pm \rho^\mp, J/\psi \eta \omega$
$\alpha/(4\sqrt{3})$	$\eta \omega \omega, \eta D^{*0} \bar{D}^{*0}, \eta D^{*+} \bar{D}^{*-}, \omega D^0 \bar{D}^0, \omega D^0 \bar{D}^{*0}, \omega D^\pm \bar{D}^{*\mp}$
$\alpha/(2\sqrt{6})$	$\eta_c D^{*0} \bar{D}^{*0}, \eta_c D^{*+} \bar{D}^{*-}, \eta_c J/\psi J/\psi$ $J/\psi D^0 \bar{D}^{*0}, J/\psi \bar{D}^0 D^{*0}, J/\psi D^\pm \bar{D}^{*\mp}$
$\alpha/4$	$\pi^0 D^{*0} \bar{D}^{*0}, \pi^0 D^{*+} \bar{D}^{*-}, \rho^0 D^0 \bar{D}^0, \rho^0 \bar{D}^0 D^0, \rho^0 D^\pm \bar{D}^{*\mp}$
$\alpha/(2\sqrt{2})$	$\rho^+ D^0 \bar{D}^{*-}, \rho^- \bar{D}^0 D^{*+}, \rho^+ D^- \bar{D}^{*0}, \rho^- D^+ \bar{D}^{*0}$

Table 1: Coupling constants for the charmed three-meson vertices within the SU(4) scheme.  $\alpha = g_a^2 N_c / (16\pi^2 F_\pi)$ .

Using the formulas developed in Section 2.8 we can write all the specific coupling constants in terms of the universal couplings  $g$  and  $g_a$ . The SU(4) scheme is shown in Table 1, with the help of which we can relate all the coupling constants of charged states among themselves. Therefore, using one known coupling constant, such as, for example the experimentally measured  $g_{D^{*+} D^0 \pi^-}$ , we can infer all the others. The couplings determined in this way are already enough to be used as input in the Lagrangians (40) - (47), which are then used in calculations of phenomenological interest. However, in the literature, one often finds a “generic” coupling constant, i.e. without any charge specification, such as, for example  $g_{D^* D \pi}$ . The choice of the generic  $g_{D^* D \pi}$  (among the the possible charged state couplings  $g_{D^{*+} D^0 \pi^-}$ ,  $g_{D^{*0} D^0 \pi^0}$ , ...etc) is a matter of convention, as mentioned explicitly in [3]. For the purpose of comparison we define the generic coupling as follows. If there is an isovector meson in the vertex, the generic coupling is the one with a neutral isovector. For example:

$$g_{D^* D \pi} = g_{D^{*\pm} D^\mp \pi^0} = g_{D^{*0} D^0 \pi^0}$$

From Table 1 the generic coupling can be obtained from the states with the charged isovector:

$$g_{D^* D \pi} = \frac{1}{\sqrt{2}} g_{D^{*-} D^0 \pi^+} = \frac{1}{\sqrt{2}} g_{D^{*+} D^0 \pi^-}$$

If there is no isovector in the vertex, all the states have the same coupling and there is no ambiguity. Then, for example:

$$g_{J/\psi DD} = g_{J/\psi D^0 D^0} = g_{J/\psi D^+ D^-}$$

All the calculations discussed throughout this review were performed for charged isovector currents.

In the next section we shall discuss in more detail the criteria which must be satisfied by the sum rules, in order to be reliable.

## 3 Evaluation of the sum rules

### 3.1 Numerical inputs

In the following subsections we will present numerical results. In the quantitative aspect, QCDSR is not like a model which contains free parameters to be adjusted by fitting experimental data. The inputs for numerical evaluations are the following: *i*) the vacuum matrix elements of composite operators involving quarks and gluons which appear in the operator product expansion (3). These numbers, known as condensates, contain all the non-perturbative component of the approach. They could, in principle, be calculated in lattice QCD. In practice they are estimated phenomenologically. They are universal and, once adjusted to fit, for example, the mass of a particle, they must have always that same value. They are the analogue for spectroscopy of the parton distribution functions in deep inelastic scattering [1]; *ii*) quark masses, which are extracted from many different phenomenological analyses; *iii*) the threshold parameter  $s_0$  is the energy (squared) which characterizes the beginning of the continuum, as shown in (8). Typically the quantity  $\sqrt{s_0} - m$  (where  $m$  is the mass of the ground state particle) is the energy needed to excite the particle to its first excited state with the same quantum numbers. This number is not well known, but should lie between 0.3 and 0.8 GeV. If larger deviations from this interval are needed, the calculation becomes suspicious. All in all, in QCDSR we do not have much freedom for choosing numbers. In the calculations discussed below we will use the numerical inputs shown in Table 2. The masses and decay constants are taken from the literature [34]. They might also be calculated with QCDSR as discussed in previous subsections.

Parameter	Value
$m_c$ (GeV)	$1.27 \pm 0.1$
$m_D$ (GeV)	1.86
$m_{D^*}$ (GeV)	2.01
$m_\rho$ (GeV)	0.775
$m_\psi$ (GeV)	3.1
$f_{J/\psi}$ (GeV)	$0.405 \pm 0.015$
$f_{D^*}$ (GeV)	$0.24 \pm 0.02$
$f_D$ (GeV)	$0.18 \pm 0.02$
$f_\rho$ (GeV)	$0.160 \pm 0.005$
$f_\pi$ (GeV)	$0.131 \pm 0.001$
$\langle \bar{q}q \rangle$ (GeV) <sup>3</sup>	$(-0.23 \pm 0.01)^3$
$\langle g^2 G^2 \rangle$ (GeV) <sup>4</sup>	$0.88 \pm 0.3$

Table 2: Parameters used in the calculation with their errors.

### 3.2 Borel stability

As it was mentioned above we perform two Borel transforms introducing the two Borel masses  $M^2$  and  $M'^2$ . The sum rules, expressing the interesting quantities as a function of the Borel parameters,

must be as much independent of these parameters as possible. An extensive check of this dependence has been carried out in [16, 17, 18, 19, 20, 21, 22, 23, 24]. For the sake of illustration we present below some numerical analysis taking the vertex  $J/\psi D^* D$  as working example. For the continuum thresholds we have used  $s_0 = (m_\psi + \Delta_s)^2$  and  $u_0 = (m_{D(D^*)} + \Delta_u)^2$  for the sum rule where  $D(D^*)$  is off-shell, and  $s_0 = (m_{D^*} + \Delta_s)^2$  and  $u_0 = (m_D + \Delta_u)^2$  for the sum rule where  $J/\psi$  is off-shell. We take  $\Delta_s = \Delta_u = (0.5 \pm 0.1)$  GeV. We first discuss the  $J/\psi DD^*$  form factor with an off-shell  $D^*$  meson.

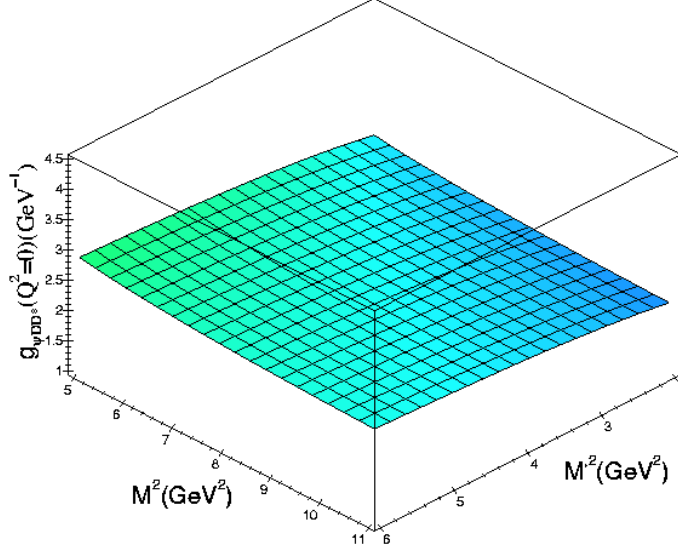


Figure 3:  $M^2$  and  $M'^2$  dependence of  $g_{\psi DD^*}^{(D^*)}(Q^2 = 0)$ .

Fixing  $Q^2 = -q^2 = 0$  and  $\Delta_s = \Delta_u = 0.5$  GeV we show in Fig. 3 the Borel dependence of the form factor  $g_{\psi DD^*}^{(D^*)}(0)$ . We see that we get a very good stability for the form factor as a function of the two independent Borel parameters in the considered Borel regions.

Since the dependence of the form factor on  $M^2$  and  $M'^2$  is weak, there is no need to continue our analysis with these two independent variables. We can relate one to another and use only one variable. One commonly used relation is:

$$\frac{M'^2}{M^2} = \frac{m_{M_1}^2}{m_{M_2}^2}, \quad (52)$$

where  $M_1$  and  $M_2$  are the mesons with  $P^2 = -p^2 \rightarrow M^2$  and  $P'^2 = -p'^2 \rightarrow M'^2$  respectively. If the meson  $M_1$  is light and the meson  $M_2$  is heavy, the above equation is replaced by:

$$\frac{M'^2}{M^2} = \frac{m_{M_1}^2}{(m_{M_2}^2 - m_c^2)}. \quad (53)$$

Other relations between  $M^2$  and  $M'^2$  are possible, such as:

$$M'^2 = aM^2 + b. \quad (54)$$

In [35] a comparative analysis was performed leading to the conclusion that all these forms are acceptable. In what follows we will discuss results obtained with (52) and with (53). We show, in Fig. 4, the behavior of the form factors  $g_{J/\psi DD^*}(Q^2)$  at  $Q^2 = 2$  GeV<sup>2</sup> as a function of the Borel mass  $M'^2$ . The solid line gives  $g_{J/\psi DD^*}^{(D^*)}$  at a fixed ratio  $M'^2/M^2 = m_D^2/m_\psi^2$ . The dashed line gives  $g_{J/\psi DD^*}^{(D)}$  at a fixed ratio  $M'^2/M^2 = m_{D^*}^2/m_\psi^2$ , and the dotted line gives  $g_{J/\psi DD^*}^{(J/\psi)}$  at a fixed ratio  $M'^2/M^2 = m_D^2/m_{D^*}^2$ . We can

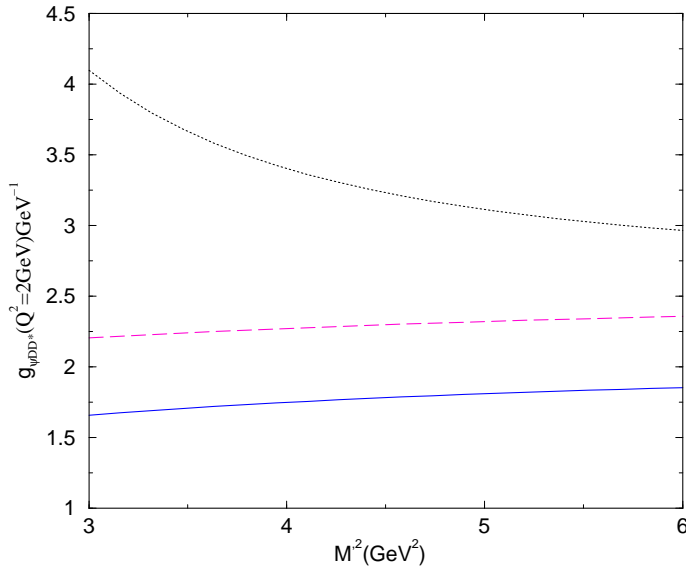


Figure 4:  $M'^2$  dependence of  $g_{J/\psi DD^*}^{(D*)}$  (solid line),  $g_{J/\psi DD^*}^{(D)}$  (dashed line) and  $g_{J/\psi DD^*}^{(J/\psi)}$  (dotted line) for  $Q^2 = 2.0 \text{ GeV}^2$ .

see that the QCDSR results for  $g_{J/\psi DD^*}^{(D*)}$  and  $g_{J/\psi DD^*}^{(D)}$  are very stable in the interval  $3 \leq M'^2 \leq 6 \text{ GeV}^2$ . In the case of  $g_{J/\psi DD^*}^{(J/\psi)}$  the stability is not as good as for the other form factors, but it is still acceptable.

### 3.3 OPE convergence

As mentioned in the previous sections the operator product expansion should always be convergent. However sometimes this convergence is not so fast. In this section we present some examples, encountered in our calculations, which illustrate extreme cases ranging from a very fast convergence, where the second term is already negligible, to a slower convergence. Fortunately, in these latter cases, the obtention of a very weak dependence of the form factor on the Borel mass (i.e., the occurrence of a stability “plateau”) indicates that the sum rule is still enough convergent.

In Fig. 5 we show the perturbative (dashed line) and the gluon condensate (dotted line) contributions to the form factor  $g_{J/\psi DD^*}^{(D*)}(Q^2)$  at  $Q^2 = 2 \text{ GeV}^2$  as a function of the Borel mass  $M'^2$  at a fixed ratio  $M'/M^2 = m_D^2/m_\psi^2$ . We see that the gluon condensate contribution is negligible, when compared with the perturbative contribution. The same kind of stability is obtained for other values of  $Q^2$  and for the other two form factors [22, 36]. In Fig. 6 we show another example of OPE behavior, now in the  $D^* D \pi$  vertex. In this Figure we study the  $D^* D \pi$  vertex, choosing the pion to be off-shell with  $Q^2 = 1 \text{ GeV}^2$  and setting  $M'^2 = M^2$ . The solid line shows the sum of the first two relevant terms of the OPE, the perturbative term and the gluon condensate. It is reassuring to observe that the former is much larger than the latter and also that their sum is very flat over a wide range of values of  $M^2$ . Although here the dominance of the perturbative term over the gluon condensate is less pronounced, we observe an interesting feature, namely, that the inclusion of the gluon condensate contributes to the Borel stability of the sum rule [16, 19]. In Figs. 7 and 8 we show a comparison between the perturbative term and quark condensate term. They illustrate how small (Fig. 7) and how large (Fig. 8) the effects of the quark condensate can be.



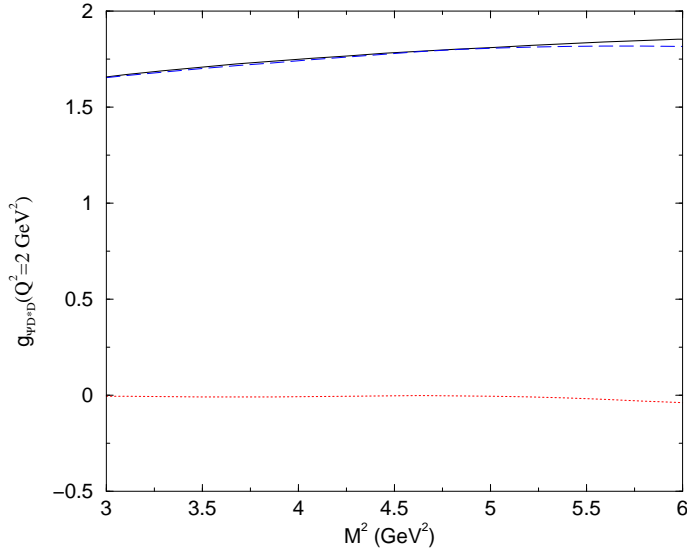


Figure 5:  $M'^2$  dependence of perturbative contribution (dashed line) and the gluon condensate contribution (dotted line) to  $g_{J/\psi DD^*}^{(D^*)}$  at  $Q^2 = 2.0 \text{ GeV}^2$ . The solid line gives the final result for the form factor.

### 3.4 Pole versus continuum

In the study of the two-point function a crucial assumption is the form of the spectral density, Eq. (6). Moreover, it is also crucial that the dispersion integral be dominated by the pole contribution and not by the continuum. In the case of the two-point function, if this condition is not satisfied we can not compute the mass of the particle. A similar condition must hold for the three-point function. If it is not dominated by the pole contribution, this could be an indication that there is more than one off-shell particle in the vertex. In the case of the two-point function the pole dominance can be tested with the help of (4). The pole and continuum contributions are given by:

$$\Pi(q^2)_{pole} = - \int_{s_{min}}^{s_0} ds \frac{\rho^{OPE}(s)}{q^2 - s + i\epsilon}, \quad (55)$$

$$\Pi(q^2)_{cont} = - \int_{s_0}^{\infty} ds \frac{\rho^{OPE}(s)}{q^2 - s + i\epsilon}. \quad (56)$$

We can perform a Borel transform in the above expressions and plot the relative contributions, which are given by:

$$\text{Pole} = \frac{\Pi(M^2)_{pole}}{\Pi(M^2)_{pole} + \Pi(M^2)_{cont}}, \quad (57)$$

$$\text{Continuum} = \frac{\Pi(M^2)_{cont}}{\Pi(M^2)_{pole} + \Pi(M^2)_{cont}}. \quad (58)$$

A similar analysis can be carried out for the three-point function. Starting with (19) and choosing one of the  $i$  tensor structures we can write:

$$F_{pole}^{OPE} = -\frac{1}{4\pi^2} \int_{s_{min}}^{s_0} ds \int_{u_{min}}^{u_0} du \frac{\rho^{OPE}(s, u, Q^2)}{(s - p^2)(u - p'^2)}, \quad (59)$$

$$F_{cont}^{OPE} = -\frac{1}{4\pi^2} \int_{s_0}^{\infty} ds \int_{u_0}^{\infty} du \frac{\rho^{OPE}(s, u, Q^2)}{(s - p^2)(u - p'^2)}, \quad (60)$$

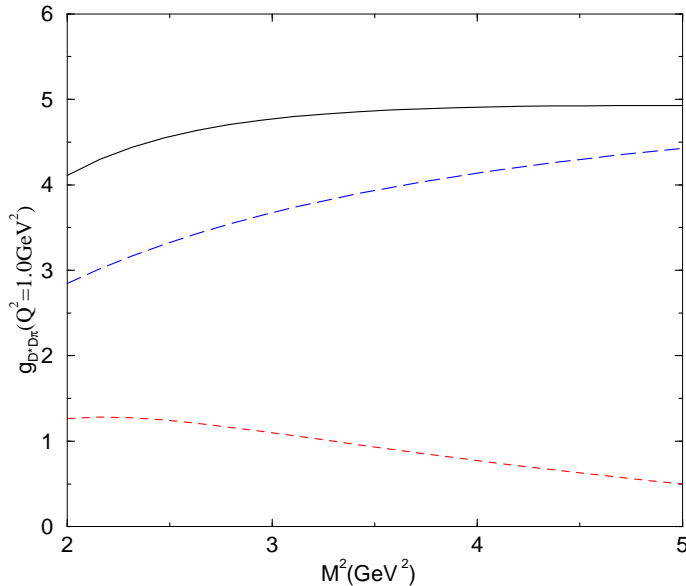


Figure 6:  $D^* D \pi$  form factor as a function of the Borel mass  $M^2$  for an off-shell pion. Dotted, dashed and solid lines represent the contribution of the gluon condensate, of the perturbative term and their sum (total) respectively.

and then, performing a double Borel transform and using (52) or (53), we write the two relative contributions as:

$$\text{Pole} = \frac{F^{OPE}(M^2)_{pole}}{F^{OPE}(M^2)_{pole} + F^{OPE}(M^2)_{cont}}, \quad (61)$$

$$\text{Continuum} = \frac{F^{OPE}(M^2)_{cont}}{F^{OPE}(M^2)_{pole} + F^{OPE}(M^2)_{cont}}. \quad (62)$$

In Figs. 9 and 10, we show the pole-continuum analysis for the  $D^* D^* \rho$  vertex [23]. In Fig. 9 the off-shell particle is the  $\rho$ , with virtuality  $Q^2 = 1 \text{ GeV}^2$ . In Fig. 10 the off-shell particle is the  $D^*$  with  $Q^2 = 1 \text{ GeV}^2$ . As it can be seen, for masses higher than  $\simeq 2.5 \text{ GeV}^2$  the sum rule is dominated by the continuum. This condition sets an upper limit for the Borel mass. A lower limit comes from imposing the OPE convergence, as it can be inferred from Fig. 6. This interval is called the “Borel window” and it does not always exist. Changing the value of  $Q^2$  may help or hinder the existence of the Borel window. In the next sections we will present QCDSR results for the form factors. We will show curves of  $g(Q^2)$  as a function of  $Q^2$  for a fixed  $M^2$ . The points where we have results are restricted to a certain region (sometimes relatively narrow) of the  $Q^2$  axis. One of the reasons for this limited range of applicability is the requirement of the pole dominance.

### 3.5 Continuum threshold effects

The results showed in Figs. 4, 5, 6, 9 and 10 were obtained using  $\Delta_s = \Delta_u = 0.5 \text{ GeV}$ . In Fig. 11 we use the form factor  $g_{J/\psi DD^*}^{(D)}(Q^2)$  to illustrate the dependence of our results on the continuum thresholds. In the Figure there are three sets of three curves. They show fits of the QCD sum rule results. The lower, intermediate and upper sets were obtained using  $\Delta_u = 0.4 \text{ GeV}$ ,  $0.5 \text{ GeV}$  and  $0.6 \text{ GeV}$  respectively. The dashed, solid and dotted lines in each set were obtained using  $\Delta_s = 0.4 \text{ GeV}$ ,  $0.5 \text{ GeV}$  and  $0.6 \text{ GeV}$  respectively. In this case we can see that the dispersion in the region  $0 \leq Q^2 \leq 4.5 \text{ GeV}^2$ , where we have the QCDSR points, does not lead to a bigger dispersion at  $Q^2 = -m_D^2$ , where the coupling constant is extracted. As it will be discussed in the next subsection, the extrapolation procedure used here does

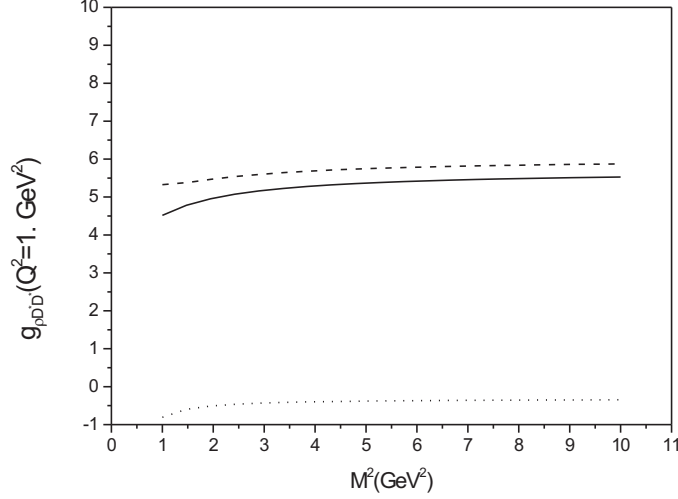


Figure 7:  $D^*D^*\rho$  form factor as a function of the Borel mass  $M^2$  for an off-shell  $D^*$ . Dotted, dashed and solid lines represent the contribution of the quark condensate, of the perturbative term and their sum (total) respectively.

not necessarily amplify the uncertainties. In fact, in some cases the uncertainties can be even damped as we move to the time-like region. An example of this damping is shown in Fig. 12, where we plot fits of the QCDSR results for the form factor of the  $D^*D\rho$  vertex. The two sets of lines correspond to a  $\rho$  off-shell (steeper lines) and to a  $D$  off-shell. Each line corresponds to a different choice of the continuum threshold parameters. As it can be seen, this is one of the major sources of uncertainties.

### 3.6 Choice of the structure

As it was discussed in the previous sections, the explicit evaluation of the correlation functions both in the OPE and in the phenomenological side leads to expressions written in terms of several tensor structures. We can write a sum rule identifying the coefficients of each structure and hence we have as many sum rules as structures. In principle all the sum rules are equivalent and should yield the same final results. In practice however, the truncation of the OPE affects different structures (and the corresponding sum rules) in different ways. Consequently some structures lead to sum rules which are more stable. In the simplest cases, such as in the  $D^*D\rho$  vertex, we have only one structure and, using the notation of (18) and (20), the correlator (both in the phenomenological and the OPE descriptions) is written as:

$$\Gamma_{\mu\nu}(p, p') = F(p^2, p'^2, q^2) \epsilon_{\alpha\beta\mu\nu} p^\alpha p'^\beta, \quad (63)$$

and an analogous expression for the OPE side. In the most complicated cases, as in the  $\rho D^*D^*$  or  $J/\psi D^*D^*$  vertices, the number of structures is fourteen and the correlators (both in the phenomenological and the OPE descriptions) have the following tensor decomposition:

$$\begin{aligned} \Gamma_{\mu\nu\alpha}(p, p') = & F_1(p^2, p'^2, q^2) g_{\mu\nu} p_\alpha + F_2(p^2, p'^2, q^2) g_{\mu\alpha} p_\nu + F_3(p^2, p'^2, q^2) g_{\nu\alpha} p_\mu \\ & + F_4(p^2, p'^2, q^2) g_{\mu\nu} p'_\alpha + F_5(p^2, p'^2, q^2) g_{\mu\alpha} p'_\nu + F_6(p^2, p'^2, q^2) g_{\nu\alpha} p'_\mu \\ & + F_7(p^2, p'^2, q^2) p_\mu p_\nu p_\alpha + F_8(p^2, p'^2, q^2) p'_\mu p_\nu p_\alpha + F_9(p^2, p'^2, q^2) p_\mu p'_\nu p_\alpha \\ & + F_{10}(p^2, p'^2, q^2) p_\mu p_\nu p'_\alpha + F_{11}(p^2, p'^2, q^2) p'_\mu p'_\nu p_\alpha + F_{12}(p^2, p'^2, q^2) p'_\mu p_\nu p'_\alpha \end{aligned}$$

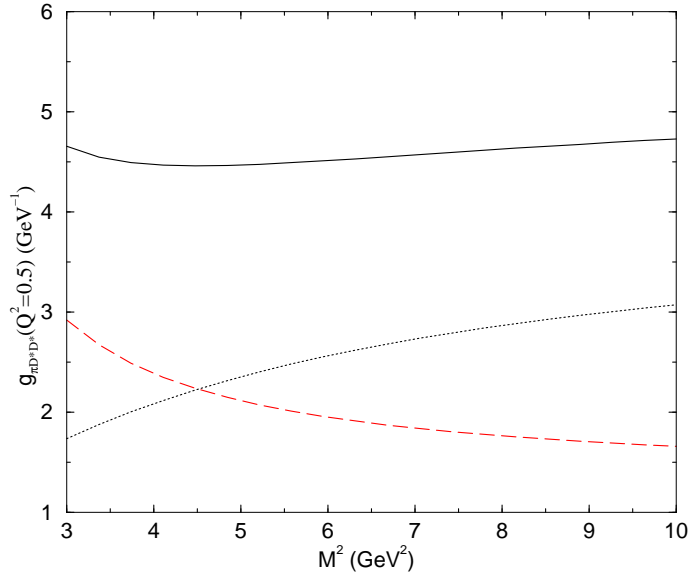


Figure 8:  $D^*D^*\pi$  form factor as a function of the Borel mass  $M^2$  for an off-shell  $D^*$ . Dashed, dotted and solid lines represent the contribution of the quark condensate, of the perturbative term and their sum (total) respectively.

$$+F_{13}(p^2, p'^2, q^2)p_\mu p'_\nu p'_\alpha + F_{14}(p^2, p'^2, q^2)p'_\mu p'_\nu p'_\alpha. \quad (64)$$

The above equation is the most general expression that can be written with three Lorentz indices  $\mu$ ,  $\nu$  and  $\alpha$ . It makes use of two independent four vectors,  $p$  and  $q$ , and the metric tensor. It contains fourteen Lorentz structures with fourteen invariant functions  $F_i$ . Although all the Lorentz structures are independent, the fourteen invariant functions can not be independent due to current conservation. Enforcing current conservation reduces the number of independent invariant functions. Usually we may take advantage of current conservation and write sum rules which are simpler. The best example is the two-point function of the vector mesons  $\rho$  and  $J/\psi$  where, instead of studying separately the two possible independent structures  $g_{\mu\nu}$  and  $q_\mu q_\nu$ , we may use a combination of them which is manifestly conserved:

$$\Pi_{\mu\nu}(q) = \Pi(q^2)(-g_{\mu\nu}q^2 + q_\mu q_\nu), \quad (65)$$

since  $q^\mu \Pi_{\mu\nu} = 0$ . The sum rule is thus written for the scalar function  $\Pi(q^2)$ . In spite of technical advantages of using (65), we may still choose to work with one single structure, either  $g_{\mu\nu}$  or  $q_\mu q_\nu$ . In the case of (64) current conservation yields identities such as

$$p^\mu \Gamma_{\nu\alpha\mu}(p, p') = 0, \quad (66)$$

or

$$p'^\alpha \Gamma_{\nu\alpha\mu}(p, p') = 0, \quad (67)$$

depending on the momentum of the  $J/\psi$  or  $\rho$  meson. With the help of expressions (66) or (67) we might rewrite the sum rules in terms of combinations of different structures. However there is nothing wrong in working with individual Lorentz structures, as done in [20] and [23].

In Fig. 13 we show the typical difference between results obtained with different structures. In the Figure we see the form factors of the  $\rho DD$  vertex, where we have only two structures  $p_\mu$  and  $p'_\mu$ . The dashed line shows the case of an off-shell  $\rho$  meson. In this case the two structures give the same result. The solid and dot-dashed lines refer to the case of an off-shell  $D$  meson and they show the same quantity computed in the two different structures. We can observe a clear difference between the two

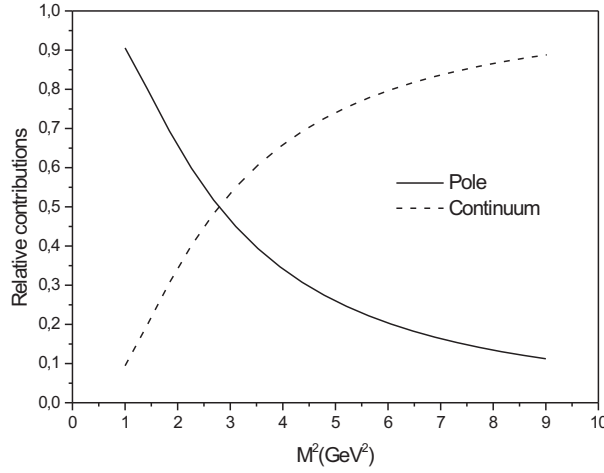


Figure 9: Pole (solid line) and continuum (dashed line) contribution to  $g_{\rho D^* D^*}^{(\rho)}(Q^2 = 1 \text{ GeV}^2)$ , as a function of the Borel mass  $M^2$ .

lines, especially in the low Borel mass region. Therefore the choice of structures deserves attention, since it may be an additional source of uncertainties. In Fig. 14 we show the form factors of the  $J/\psi D^* D^*$  vertex for fixed  $M^2$  as a function of  $Q^2$ . The dashed and dotted lines show results obtained with different structures.

## 4 Form factors

In the previous section we have presented the conditions which must be satisfied for a sum rule to be considered reliable. In this section we discuss a difficulty inherent to the calculation of coupling constants with QCDSR. The solution of (31) is numerical and restricted to a singularity-free region in the  $Q^2$  axis, usually located in the space-like region. Therefore, in order to reach the pole position,  $Q^2 = -m_{M_3}^2$ , we must fit the solution, finding a function  $g_{M_1 M_2 M_3}^{(M_3)}(Q^2)$  which is then extrapolated to the pole, yielding the coupling constant. In the following subsections we introduce an extrapolation procedure and discuss how to improve it.

### 4.1 The extrapolation procedure

In order to minimize the uncertainties associated with the extrapolation procedure, for each vertex we perform the calculation twice, putting first one meson and then another meson off-shell, obtaining two form factors  $g_{M_1 M_2 M_3}^{(M_1)}(Q^2)$  and  $g_{M_1 M_2 M_3}^{(M_2)}(Q^2)$  and requiring that these two functions have the same value at the respective poles. The superscripts in parenthesis indicate which meson is off-shell.

In order to yield reliable results the sum rule (31) must satisfy the quality criteria discussed in the previous subsections. In first place (31) is a function of two Borel masses  $M^2$  and  $M'^2$ . A good sum rule is independent of the choice of these masses (it is “Borel stable”), showing a plateau when plotted as a function of  $M^2$  or  $M'^2$ . Moreover, the OPE side is a series which must be convergent. We choose a value for  $M^2$  and plot (31) as a function of  $Q^2$ , as it is shown in Fig. 15. The squares and circles show the result of the numerical evaluation of the form factor  $g(Q^2)$  as a function of  $Q^2$  for the  $D^* D \pi$  vertex with a pion (squares) and a  $D$  (circles) off-shell. As it can be seen, at a certain (low) value of  $Q^2$  the calculation stops, because at this point the stability and convergence criteria are no longer satisfied.

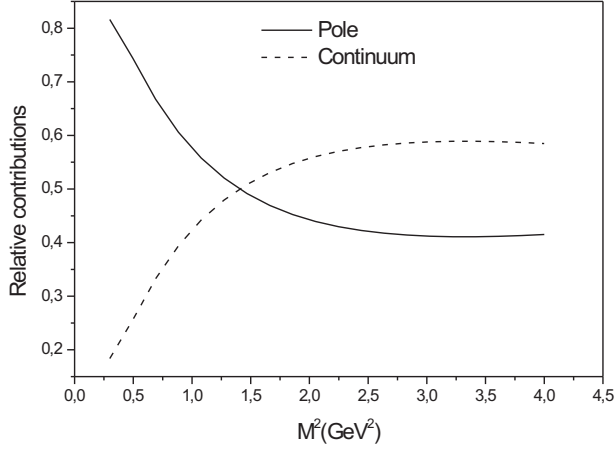


Figure 10: Pole versus continuum contributions to  $g_{\rho D^* D^*}^{(D^*)}(Q^2 = 1 \text{ GeV}^2)$  as a function of the Borel mass  $M^2$ .

From here on we have to extrapolate. In Fig. 15 we show fits of the QCDSR results represented by the lines. As it is illustrated in the case of an off-shell pion, the numerical points obtained with QCDSR can be fitted, with similar accuracy, by several forms which, when extrapolated to  $Q^2 = -m_\pi^2$ , will lead to very different points! This can be clearly seen by comparing the dashed and dash-dotted lines in Fig. 15. In order to reduce the freedom in the extrapolation and constrain the form factor we calculate and fit simultaneously the values of  $g(Q^2)$  of the same  $D^* D \pi$  vertex with the  $D$  off-shell. The results are shown in Fig. 15 with circles fitted by the solid line. We perform the fits of the two sets of points (circles and squares) imposing the condition that *the two resulting parametrizations, when extrapolated to  $Q^2 = -m_\pi^2$  and  $Q^2 = -m_D^2$  go to the same value of  $g_{D^* D \pi}(Q^2)$* . This procedure is enough to reduce the uncertainties and, imposing this requirement leads to  $g_{D^* D \pi} = 14.0 \pm 1.5$ , which is consistent with the experimental value  $g_{D^* D \pi} = 17.9 \pm 0.3 \pm 1.9$ .

As another interesting example, we consider the vertex  $J/\psi D D^*$ . Here we try to improve the procedure described above, calculating three form factors (one for each off-shell particle). This new procedure imposes a more stringent condition on the parametrizations. Fixing  $M^2$  and  $M'^2$  to the values of the incoming and outgoing meson masses we show, in Fig. 16, the momentum dependence of the QCDSR results for the three form factors  $g_{J/\psi D D^*}^{(D)}$ ,  $g_{J/\psi D D^*}^{(D^*)}$  and  $g_{J/\psi D D^*}^{(J/\psi)}$  through the circles, squares and triangles respectively. Since our approach cannot be used at  $Q^2 \ll 0$ , in order to extract the  $g_{J/\psi D D^*}$  coupling from the form factors we extrapolate the curves to the mass of the off-shell meson, shown as open circles in Fig. 16. In order to do this extrapolation we fit the QCDSR results with an analytical expression. We tried to fit our results to a monopole form, since this is very often used for form factors, but the fit was only good for  $g_{J/\psi D D^*}^{(J/\psi)}$ . For  $g_{J/\psi D D^*}^{(D)}$  and  $g_{J/\psi D D^*}^{(D^*)}$  we obtained good fits using a Gaussian form. These fits are also shown in Fig. 16 through the dotted, solid and dashed lines respectively. From Fig. 16 we see that all three form factors lead to compatible values for the coupling constant when extrapolated to the off-shell meson masses (open circles in Fig. 16).

From the parametrizations we can also extract the cutoff parameter,  $\Lambda$ , associated with the form factors. The general expression for the Gaussian parametrization is:  $A \exp[-(Q^2 + B)^2/\Lambda^4]$ , which gives  $\Lambda \sim 4.5 \text{ GeV}$  when the off-shell meson is  $D$  or  $D^*$ . For the monopole parametrization the general expression is:  $g[(\Lambda^2 - m^2)/(\Lambda^2 + Q^2)]$ . Therefore, for an off-shell  $J/\psi$  we get  $\Lambda \sim 7.5 \text{ GeV}$ . It is very interesting to notice that the value of the cutoff is directly associated with the mass of the off-shell meson in the vertex. The form factor is harder (i.e., the curve in the Figure is flatter) if the off-shell

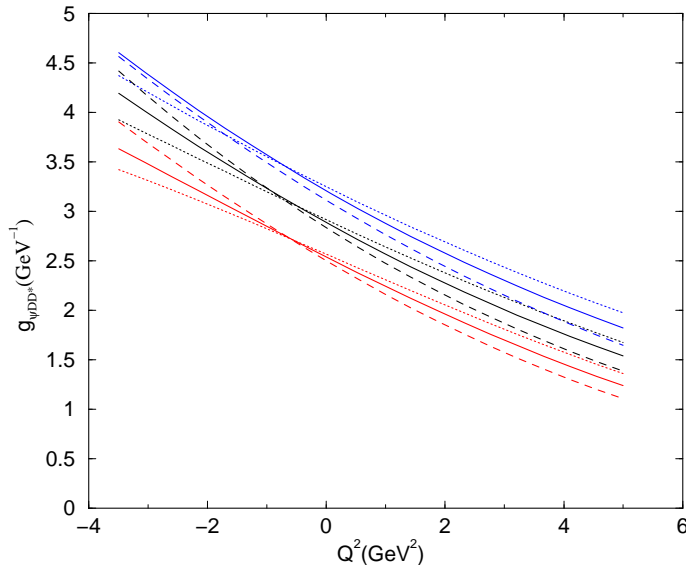


Figure 11: Continuum threshold dependence of the form factor  $g_{\psi DD^*}^{(D)}(Q^2)$ . The dashed solid and dotted lines give the parametrization of the QCDSR results for  $\Delta_s = 0.4$  GeV,  $0.5$  GeV and  $0.6$  GeV respectively. The lower, intermediate and upper set of curves show the results for  $\Delta_u = 0.4$  GeV,  $0.5$  GeV and  $0.6$  GeV respectively.

meson is heavier.

## 4.2 Hadronic loops

Coming back to the  $D^*D\pi$  vertex, we observe that, while the obtained number,  $g_{D^*D\pi} = 14.0 \pm 1.5$ , is not far from the experimental value, there is still a discrepancy. The procedure of fitting the QCDSR points in the deep euclidean region and extrapolating them to the time-like region contains systematic uncertainties associated to *the analytical form chosen for the parametrizations*, i.e., monopole, exponential or gaussian. We tried to reduce this systematic uncertainty performing a double (and also a triple as in the case of the  $J/\psi D^*D$  vertex) fit. However it would be desirable to have a more physical way to reduce the systematic uncertainty.

In [37] the authors revisited this problem, employing hadronic loops, calculated by means of effective field theories (EFT), in order to produce a better parametrization for  $D^*D\pi$  results calculated with QCDSR. Purely hadronic calculations are independent from QCDSR and involve the choice of an effective Lagrangian, including the possible requirements of chiral symmetry and/or SU(4). Beyond the tree level, one has to deal with the problems and uncertainties associated with renormalization. As it was discussed in [37] a suitable combination of EFT and QCDSR results allows the reduction of undesired indeterminacies of both approaches, improving their predictive power.

The full  $D^*D\pi$  vertex function in a hadronic approach involves the computation of several diagrams. Leading contributions to this vertex come from both the tree interaction and from the diagrams depicted in Fig. 17. Meson loops are a necessary consequence of quantum field theory and do contribute to several hadronic observables. In practice, due to problems associated with infinities, renormalization becomes unavoidable in the evaluation of loop corrections to observables. Here the basic idea is to isolate the unknown loop parameters into some basic constants, in such a way that they can be determined by matching the results of loop and QCDSR results.

We note that some diagrams, such as, for instance, that in Fig. 17 a, contain internal vertices involving the  $D^*D\pi$  coupling. This suggests that the calculation is “cyclic”, since one needs to use the

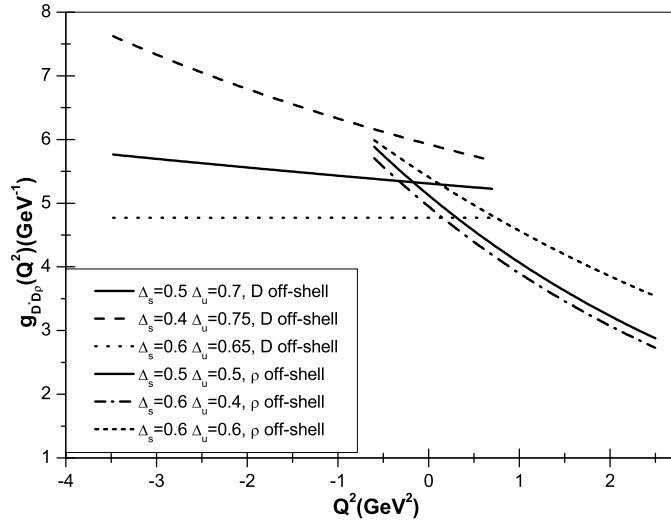


Figure 12: Dependence of the  $D^*D\rho$  form factors on the continuum thresholds. The steeper lines correspond to  $\rho$  off-shell. The others are for D off-shell.

$D^*D\pi$  form factor in order to calculate the  $D^*D\pi$  form factor. Actually, there are differences between the internal particles and the external ones. The former are always virtual, whereas the latter may be either real or put on mass shell in the extraction of the coupling constant. In the framework of perturbation theory, at leading order, internal particles are treated as elementary, without structure. They are assumed to be point-like and the evaluation of leading terms does not require the use of internal form factors. Consistently, one must use bare coupling constants for these interactions.

Since there are heavy mesons circulating in the loops shown in Fig. 17, one might argue that other states should also be included. We do have, for example, fermion-antifermion components such as  $\bar{N}N$  or  $\bar{\Lambda}_c\Lambda_c$  in the loops. An incoming positive pion can split into a  $p$  plus a  $\bar{n}$ , and so on. However, in a different context [38], it has been shown that this kind of splitting is suppressed with respect to the pion  $\rightarrow$  meson-meson splitting, by one order of magnitude. The neglect of this kind of contribution seems therefore justified. The same holds for the possibility of strangeness circulating in the loop, associated with virtual states such as  $D_s$ ,  $D_s^*$ ,  $K$  and  $K^*$ . Using only  $\pi$ 's,  $\rho$ 's,  $D$ 's and  $D^*$ 's the low and high  $Q^2$  regions of the form factor are covered. Thus it is enough to work with a simple effective theory. It is convenient to use the effective Lagrangian (40), which is constrained by SU(2) flavor and chiral symmetries, as well as gauge invariance. The coupling constant appearing in the Lagrangian is the bare one. The  $\rho$  couplings are assumed to be universal and are implemented by covariant derivatives of the form  $\mathcal{D}^\mu = \partial^\mu - ig_\rho \mathbf{T} \cdot \boldsymbol{\rho}^\mu$ , where  $g_\rho$  is the universal coupling constant and  $\mathbf{T}$  is the isospin matrix suited to the field upon which the derivative  $\mathcal{D}^\mu$  acts. With the proper Lagrangians it is possible to write and evaluate all the contributions to the total vertex function.

The  $\pi(q) D(p) D_\alpha^*(p')$  vertex function  $\Gamma_\mu(p^2)$  for an off-shell  $D$  is written as:

$$\Gamma_\mu(p^2) = -q_\mu g_{D^*D\pi}^{(D)}(p^2), \quad (68)$$

where  $g_{D^*D\pi}^{(D)}(p^2)$  is the form factor, such that the physical coupling constant is  $g_{D^*D\pi} = g_{D^*D\pi}^{(D)}(m_D^2)$ . In [37] two kinds of loop corrections to this vertex were considered, containing pion and  $\rho$  intermediate states, denoted respectively by  $F_\pi(p^2)$  and  $F_\rho(p^2)$ . The perturbative evaluation of these functions gives rise to divergent integrals and  $g_{D^*D\pi}^{(D)}(p^2)$  can be determined only up to yet unknown renormalization constants. The use of standard loop integration techniques, such as dimensional regularization and  $\overline{MS}$  subtraction of divergences, for all diagrams, allows one to write the form factor as:

$$g_{D^*D\pi}^{(D)}(p^2) = K + C_\pi F_\pi(p^2) + C_\rho F_\rho(p^2), \quad (69)$$



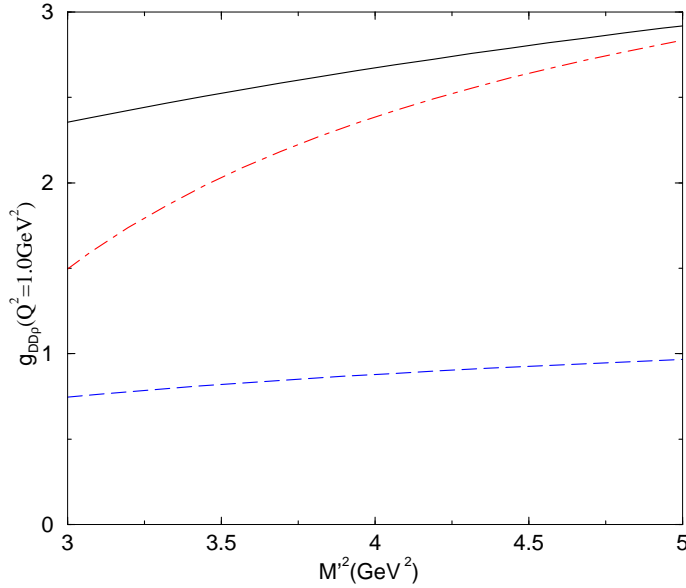


Figure 13:  $M'^2$  dependence of the  $DD\rho$  form factors at  $Q^2 = 1 \text{ GeV}^2$  for  $\Delta_s = \Delta_u = 0.5 \text{ GeV}$ . The dashed line gives the QCDSR result for  $g_{DD\rho}^{(\rho)}(Q^2)$  and the dot-dashed and solid lines give the QCDSR results for  $g_{DD\rho}^{(D)}(Q^2)$  in the  $p_\mu$  and  $p'_\mu$  structures respectively.

where  $K$ ,  $C_\pi$  and  $C_\rho$  are constants. These constants incorporate the bare couplings, the usual parameters associated with renormalization and here they are determined by comparing  $g_{D^*D\pi}^{(D)}(p^2)$  with the results from QCD sum rules. Keeping only the terms which depend on  $p^2$  the explicit evaluation of the diagrams can be performed and the form factor as a function of  $p^2$ , the  $D$  four-momentum squared, can be obtained. At this stage, it still contains three unknown parameters, which are determined by adjusting the function  $g_{D^*D\pi}^{(D)}(p^2)$  to the QCD sum rule points taken from [19]. Those results are displayed in Fig. 18, where  $P^2 = -p^2$ , together with the best fit ( $\chi^2 \sim 10^{-3}$ ) represented by the solid line. Computing the value of  $g_{D^*D\pi}^{(D)}(p^2)$  at  $p^2 = m_D^2$ , one arrives at the following value for the coupling constant:

$$g_{D^*D\pi} = 17.5 \pm 1.5, \quad (70)$$

in very good agreement with experiment. The errors quoted come from the QCDSR points, which contain a typical error of  $\simeq 10 \%$ . In the same Figure we can also see the results of the fits of the QCDSR points with two mixed monopole-dipole structures with three free parameters, namely:

$$g^I(p^2) = C \left[ \frac{\Lambda_1^2 - m_D^2}{\Lambda_1^2 - p^2} + \left( \frac{\Lambda_2^2 - m_D^2}{\Lambda_2^2 - p^2} \right)^2 \right], \quad (71)$$

$$g^{II}(p^2) = C_1 \frac{\Lambda^2 - m_D^2}{\Lambda^2 - p^2} + C_2 \left( \frac{\Lambda^2 - m_D^2}{\Lambda^2 - p^2} \right)^2, \quad (72)$$

which yield  $\chi_I^2 \sim 10^{-3}$  (dashed line) and  $\chi_{II}^2 \sim 10^{-2}$  (dash-dotted line), respectively. Looking at Fig. 18 we learn that these alternative structures, reasonable as they are, diverge significantly from the loop calculation in the region where the  $D$  is not too off-shell, stressing the importance of a proper hadronic treatment of the form factor in that region.

As far as practical applications are concerned, our numerical results for the form factor  $g_{D^*D\pi}(p^2)$ , in the whole range  $-m_D^2 \leq P^2 < 5 \text{ GeV}^2$ , are very well described by the mixed monopole-dipole structure given by Eq. (71) with the parameters  $C = 8.7$ ,  $\Lambda_1 = 5.1 \text{ GeV}$  and  $\Lambda_2 = 2.9 \text{ GeV}$ . These results suggest

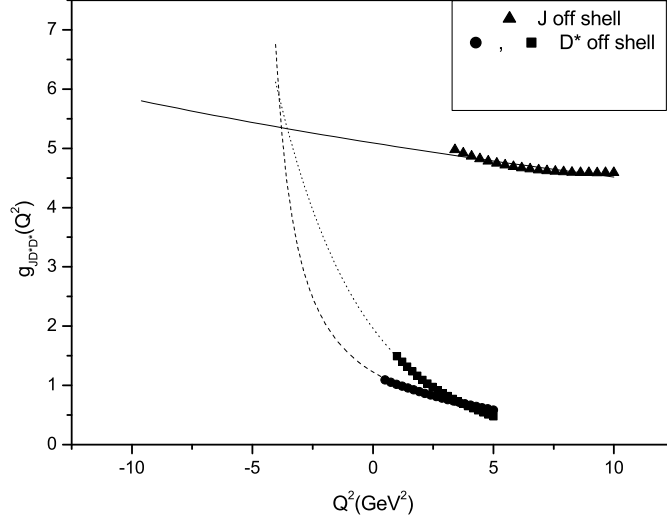


Figure 14:  $g_{J/\psi D^* D^*}^{(D^*)}$  (circles and squares) and  $g_{J/\psi D^* D^*}^{(J/\psi)}$  (triangles) form factors as a function of  $Q^2$  from the QCDSR calculation of this work. The solid and dashed lines correspond to the monopole parametrization of the QCDSR data, using two different structures, and the dotted line corresponds to the exponential parametrization.

that the use of meson loops can reduce the uncertainty in the extrapolation of form factors, computed in the space-like region by means of QCDSR, to the time-like region, with the corresponding increase in the reliability of predictions for coupling constants. Apart from the approximations described above, the procedure has no new source of errors.

To conclude this section, we have discussed a new method of improving QCDSR calculations of hadronic form factors, which consists in matching QCDSR results, valid mainly in the deep euclidean region, to meson loop calculations, valid when the  $D$  is not too off-shell. This matching is well justified from the physical point of view, since in the intermediate and large  $Q^2$  regions the relevant degrees of freedom are the quarks and gluons, with non-perturbative corrections taken into account through the QCD condensates. The opposite happens for low values of  $Q^2$ , where sum rules calculations become non-reliable due to the lack of a large mass scale. At this point, the meson exchange dynamics becomes a reliable tool, but it depends on unknown constants associated with the renormalization of the mesonic vertices. Although the exact frontier between meson dynamics and QCDSR cannot be precisely known, the success of the method in the example considered here supports the view that the matching may become useful in increasing the predictive power of both procedures.

## 5 Results

### 5.1 Form factors and couplings

We have applied the procedure described in the previous sections to the following vertices  $D^* D \pi$ ,  $D^* D^* \pi$ ,  $DD\rho$ ,  $D^* D \rho$ ,  $D^* D^* \rho$ ,  $J/\psi DD$ ,  $J/\psi D^* D$  and  $J/\psi D^* D^*$ . As mentioned above, for each vertex we obtain two sets of points, which have been parametrized by the following forms:

$$(I) \quad g_{M_1 M_2 M_3}^{(M_i)} = \frac{A}{Q^2 + B} \quad (73)$$

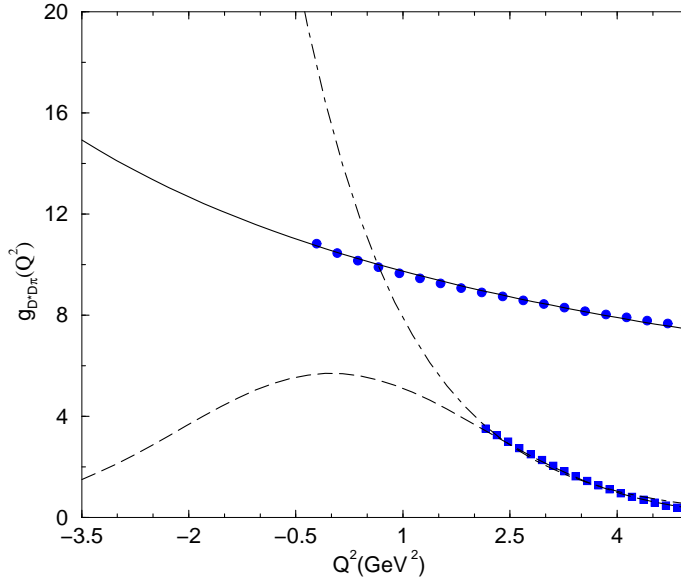


Figure 15:  $D^*D\pi$  form factor as a function of  $Q^2$  for an off-shell pion (dashed and dot-dashed lines) and an off-shell  $D$  (solid line). Circles and squares are the results of numerical calculations and the curves are their fits.

$$(II) \quad g_{M_1 M_2 M_3}^{(M_i)} = A \exp[-(Q^2/B)] \quad (74)$$

$$(III) \quad g_{M_1 M_2 M_3}^{(M_i)} = A \exp[-(Q^2 + C)^2/B]. \quad (75)$$

In Table 3 each line refers to the vertex indicated in the first column. In the second, third and fourth columns we present the values of the parameters A and B for the case where a heavier meson in the vertex ( $M_1$ ) is off-shell, indicating also which parametrization ((I), (II) or (III)) was employed. In the fifth, sixth, seventh and eighth columns we show the parameters and type of parametrization used in the case where a lighter meson ( $M_2$ ) is off-shell. The numbers presented in Table 4 summarize our

$M_1 M_2 M_3$	Form	$M_1$ off		Form	$M_2$ off		
		A	B		A	B	C
$D\pi D^*$	(I)	126	11.9	(II)	15.5	1.48	
$J/\psi DD^*$	(I)	200	57	(III)	13	450	26
$J/\psi DD$	(I)	306	63	(III)	15	250	20
$D\rho D$	(I)	37.5	12.1	(II)	2.5	0.98	
$J/\psi D^* D^*$	(I)	400	78.5	(II)	1.96	3.5	
$D^* \rho D^*$	(II)	4.9	13.3	(II)	5.2	2.7	
$D^* \pi D^*$	(II)	4.8	6.8	(II)	8.5	3.4	
$D\rho D^*$	(I)	234	44	(II)	5.1	4.3	

Table 3: Parameters used in (73), (74) and (75). B and C are in  $\text{GeV}^2$  and A is either in GeV or  $\text{GeV}^2$ , depending on the vertex. All the isovector mesons  $\pi$  and  $\rho$  appearing in the Table are charged.

results. They contain uncertainties coming from different sources, which will be discussed in the next section. The vertex coupling constants can be obtained from the form factors and they are presented in Table 4. A comparison with other estimates is going to be done in section 6.

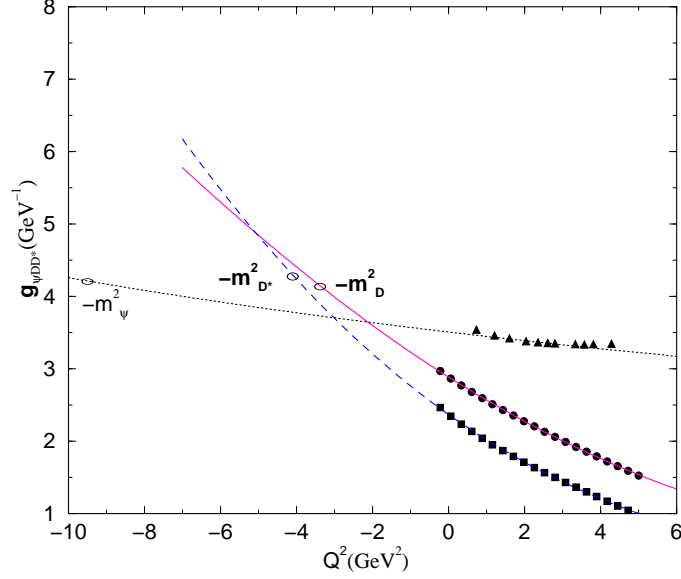


Figure 16: Momentum dependence of the  $J/\psi DD^*$  form factors. The dotted, dashed and solid lines give the parametrization of the QCDSR results (triangles, squares and circles).

$M_1 M_2 M_3$	$g_{M_1 M_2 M_3}$
$D\pi D^*$	$9.9 \pm 1.0$
$J/\psi DD^*$	$4.0 \pm 0.6 \text{ GeV}^{-1}$
$J/\psi DD$	$5.8 \pm 0.9$
$D\rho D$	$3.0 \pm 0.2$
$J/\psi D^* D^*$	$6.2 \pm 0.9$
$D^* \rho D^*$	$4.7 \pm 0.2$
$D^* \pi D^*$	$6.1 \pm 0.7 \text{ GeV}^{-1}$
$D\rho D^*$	$4.3 \pm 0.9 \text{ GeV}^{-1}$

Table 4: Coupling constants for neutral isovector mesons ( $\pi^0$  and  $\rho^0$ ).

## 5.2 Uncertainties

We consider now, as an example, the vertex  $D^* D \rho$  and discuss, one by one, all the sources of uncertainties in the calculation of the form factors. The sum rules for  $D$ ,  $\rho$  and  $D^*$  off-shell are given by:

$$C \frac{g_{D^* D \rho}^{(D)}}{(Q^2 + m_D^2)} e^{-\frac{m_D^2}{M'^2}} e^{-\frac{m_{D^*}^2}{M^2}} = -\frac{1}{4\pi^2} \int ds \int du \rho^{(D)}(u, s, t) e^{-\frac{s}{M^2}} e^{-\frac{u}{M'^2}} - \langle \bar{q}q \rangle e^{-m_c^2/M^2}, \quad (76)$$

$$C \frac{g_{D^* D \rho}^{(\rho)}}{(Q^2 + m_\rho^2)} e^{-\frac{m_D^2}{M'^2}} e^{-\frac{m_{D^*}^2}{M^2}} = -\frac{1}{4\pi^2} \int ds \int du \rho^{(\rho)}(u, s, t) e^{-\frac{s}{M^2}} e^{-\frac{u}{M'^2}}, \quad (77)$$

and

$$C \frac{g_{D^* D \rho}^{(D^*)}}{(Q^2 + m_{D^*}^2)} e^{-\frac{m_D^2}{M'^2}} e^{-\frac{m_\rho^2}{M^2}} = -\frac{1}{4\pi^2} \int ds \int du \rho^{(D^*)}(u, s, t) e^{-\frac{s}{M^2}} e^{-\frac{u}{M'^2}} + \langle \bar{q}q \rangle e^{-m_c^2/M^2}, \quad (78)$$

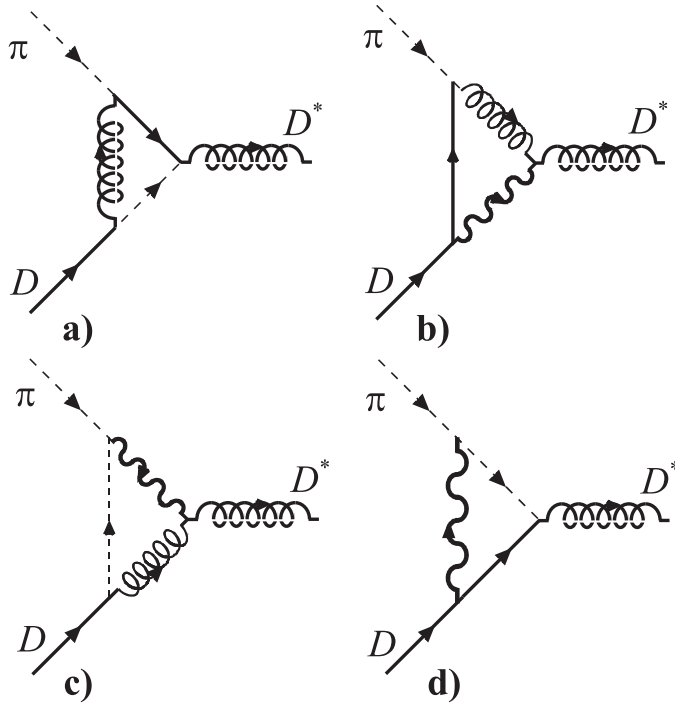


Figure 17: Meson loop contributions to the  $D^*D\pi$  form factor: “triangle” diagrams. In the internal triangles the solid, dashed, wavy and spring lines represent a virtual  $D$ ,  $\pi$ ,  $\rho$  and  $D^*$  respectively.

where  $t = -Q^2$  and the functions  $\rho^{(D)}$ ,  $\rho^{(\rho)}$  and  $\rho^{(D^*)}$  are the double discontinuities associated to the perturbative diagram of the sum rules with an off-shell  $D$ ,  $\rho$  and  $D^*$  off-shell respectively. They are given by:

$$\rho^{(D)}(u, s, t) = \frac{3m_c}{\sqrt{\lambda}} \left[ \frac{u(2m_c^2 - s - t + u)}{\lambda} \right], \quad (79)$$

with  $\lambda = (u + s - t)^2 - 4us$ . The integration limits in (76) are:

$$0 < u < \frac{m_c^2(s + t - m_c^2) - st}{m_c^2},$$

and

$$m_c^2 < s < s_0,$$

The perturbative contribution for the double discontinuity for an off-shell  $\rho$  meson is given by:

$$\rho^{(\rho)}(u, s, t) = \frac{3m_c t}{\lambda^{3/2}} \left[ u + s - t - 2m_c^2 \right], \quad (80)$$

and the corresponding integration limits in (77) are:

$$\frac{m_c^2(s - t - m_c^2)}{s - m_c^2} < u < u_0,$$

and

$$m_c^2 < s < s_0,$$

The perturbative contribution for the double discontinuity for an off-shell  $D^*$  meson is given by:

$$\rho^{(D^*)}(u, s, t) = \frac{3m_c}{\lambda^{3/2}} \left[ s(2m_c^2 + s - t - u) \right], \quad (81)$$

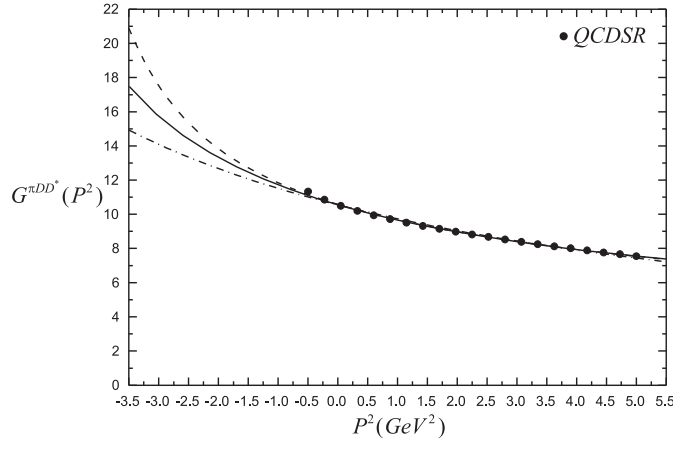


Figure 18: The  $D^* D \pi$  form factor. Dots: QCDSR from [19]; solid, dash and dash-dotted lines are fits obtained with eq. (69), (71) and (72), respectively.

The integration limits in (78) are:

$$t < u < \frac{m_c^2(t - s - m_c^2)}{t - m_c^2},$$

and

$$0 < s < s_0,$$

In the above expressions  $C$  is a constant defined as:

$$C = \frac{m_D^2 f_D}{m_c} m_\rho f_\rho m_{D^*} f_{D^*},$$

where  $f_D$ ,  $f_\rho$  and  $f_{D^*}$  are the decay constants of the mesons  $D$ ,  $\rho$  and  $D^*$  respectively. The numerical evaluation of the above expressions is done with the numerical inputs shown in Table 2 and the resulting points are shown in Fig. 19. The triangles, squares and circles are the results for the  $g_{D^* D \rho}^{(\rho)}(Q^2)$ ,  $g_{D^* D \rho}^{(D)}(Q^2)$  and  $g_{D^* D \rho}^{(D^*)}(Q^2)$  form factors respectively. As indicated in Table 3, in the case of an off-shell  $D$  meson, our numerical results can be fitted by the following monopolar parametrization (shown by the dashed line in Fig. 19):

$$g_{D^* D \rho}^{(D)}(Q^2) = \frac{234}{Q^2 + 44}, \quad (82)$$

where the function  $g_{D^* D \rho}^{(D)}(Q^2)$  has the units of  $\text{GeV}^{-1}$ . Following the procedure discussed above, we define the coupling constant as the value of the form factor at  $Q^2 = -m_M^2$ , where  $m_M$  is the mass of the meson  $M$ . Therefore, using  $Q^2 = -m_D^2$  in Eq (82), the resulting coupling constant is  $g_{D^* D \rho}^{(D)} = 5.76 \text{ GeV}^{-1}$ . For an off-shell  $\rho$  meson our sum rule results can be fitted by an exponential parametrization, which is represented by the solid line in Fig. 19:

$$g_{D^* D \rho}^{(\rho)}(Q^2) = 5.1 e^{-Q^2/4.3}. \quad (83)$$

Using  $Q^2 = -m_\rho^2$  in Eq (83) we get  $g_{D^* D \rho}^{(\rho)} = 5.89 \text{ GeV}^{-1}$ . In the case of an off-shell  $D^*$  meson, our numerical results can be fitted by the following monopolar parametrization (shown by the dotted line in Fig. 19):

$$g_{D^* D \rho}^{(D^*)}(Q^2) = \frac{195.8}{Q^2 + 33.5}. \quad (84)$$

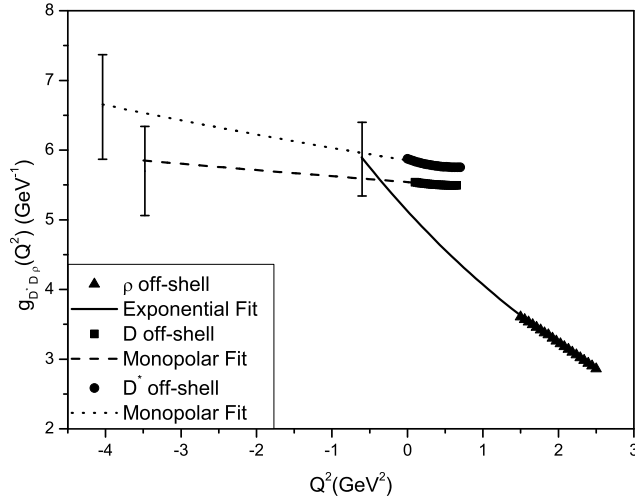


Figure 19: The  $D^*D\rho$  form factor.  $g_{D^*D\rho}^{(D)}$  (squares),  $g_{D^*D\rho}^{(\rho)}$  (triangles) and  $g_{D^*D\rho}^{(D^*)}$  (circles) form factors as a function of  $Q^2$ . The dotted, solid and dashed lines correspond to the parametrizations discussed in the text. The vertical bars show the theoretical errors in the coupling constants once all variations in the parameters are taken into account, as explained in the text.

Evaluating this form factor at  $Q^2 = -m_{D^*}^2$  we find the coupling  $g_{D^*D\rho}^{(D^*)} = 6.65 \text{ GeV}^{-1}$ .

Looking at Fig. 19 we can observe that the  $D$  off-shell form factor is much harder than the  $\rho$  off-shell one. This agrees with the behavior observed in Figs. 14, 15 and 16: the heavier is the off-shell meson, the harder is its form factor. Following this same trend, we would expect the  $D^*$  off-shell form factor to be even harder than the  $D$  off-shell one. However, comparing the dashed and dotted lines in Fig. 19, this seems not to be the case: the slope of the  $D^*$  curve is slightly bigger than the one of the  $D$  curve. Since their mass difference is relatively small ( $\simeq 150 \text{ MeV}$ ) the two curves should have almost the same slope. The observed difference is an indication of the limited precision of our method.

The form factors (82), (83), (84) and their extrapolations to the on-shell points leading to the coupling constants do not contain error bars. In fact, a careful and systematic study of errors in QCDSR calculations is hard to find in the literature. We took Refs. [39] as a guide. In Fig. 19 we can see the theoretical error bars at the endpoints of the three curves. In what follows we describe how we obtain them. First, we compute the sum rules (76), (77) and (78) extensively, taking into account the errors in the masses, decay constants, condensates, choice of the Borel mass and continuum threshold parameters. In each computation all the parameters are kept fixed, except one, which is changed according to its intrinsic error. The errors in the quark and gluon condensates, in the masses and decay constants are listed in Table 2. The three Borel masses were chosen in the interval  $2.7 \leq M^2 \leq 3.3 \text{ GeV}^2$  for an off-shell  $\rho$  and an off-shell  $D^*$  and in the interval  $27 \leq M^2 \leq 33 \text{ GeV}^2$  for an off-shell  $D$ . After each round of calculation of the three sum rules, we obtain three sets of points which are then fitted and extrapolated to the respective on-shell points. The sets of points are all fitted with the forms (82), (83) and (84), but for each set the numerical constants appearing in these forms are different.

Every extrapolation introduces some ambiguity in the final results, since we have the freedom to fit a set of points with different parametrizations. In our case this freedom is strongly reduced because we require that all the three parametrizations lead to approximately the same coupling constant. In Fig. 19 this requirement forces the three endpoints of (82), (83) and (84), which are taken at the squared masses of the corresponding particles, to coincide, i.e., to have approximately the same height in the

Quantity	$\langle g_{D^*D\rho}^{(\rho)} \rangle$	$\sigma$	$\sigma$ (%)
$\Delta$	5.86	0.08	1.4
$f_\rho$	5.89	0.01	0.1
$f_D$	5.41	0.65	12.0
$f_{D^*}$	5.90	0.40	6.8
$M^2$	5.90	0.10	1.7
$m_c$	5.97	0.40	7.4

Table 5: Changes in  $g_{D^*D\rho}^{(\rho)}$  induced by changes in different quantities.

figure. Of course, due to the approximations used, we can not expect this matching to be perfect. Once this procedure is completed and we determine the three coupling constants with an error corresponding solely to the variation of one parameter, we move to the next parameter to be varied, keeping all others fixed and repeat the procedure. In each step we can have an idea of how sensitive is each coupling constant to the parameter under consideration. In the end, for each coupling constant we take the average of all encountered values and calculate also the global error, which is shown in Fig. 19 as an error bar at the on-shell point. The final number is then obtained taking the average of the three couplings found and the final error is also obtained from the errors of each coupling.

Among the sources of errors, one deserves a special discussion. Very often in QCDSR calculations, appreciable uncertainties in the results come from the lack of knowledge on the continuum threshold parameters. In order to study the dependence of our results on these parameters, we vary  $\Delta_{s,u}$  between  $0.4 \text{ GeV} \leq \Delta_{s,u} \leq 0.6 \text{ GeV}$  in the sum rule (77), between  $0.4 \text{ GeV} \leq \Delta_s \leq 0.6 \text{ GeV}$  and  $0.65 \text{ GeV} \leq \Delta_u \leq 0.75 \text{ GeV}$  in the sum rule (76) and between  $0.65 \text{ GeV} \leq \Delta_s \leq 0.75 \text{ GeV}$  and  $0.50 \text{ GeV} \leq \Delta_u \leq 0.70 \text{ GeV}$  in the sum rule (78). This variation produces new sets of curves which are shown in Fig. 12 and give us an uncertainty range in the resulting coupling constants  $g_{D^*D\rho}^{(D)}$  and  $g_{D^*D\rho}^{(\rho)}$ . For the sake of clarity we did not include the lines corresponding to the coupling  $g_{D^*D\rho}^{(D^*)}$ . Surprisingly, in the case of the form factor  $g_{D^*D\rho}^{(\rho)}$ , we observe a convergence of the extrapolation lines, which reduces the final error. Due to this accident, the continuum threshold parameters are not, in the  $g_{D^*D\rho}^{(\rho)}$  case, the ultimate source of error. Their contribution (denoted by  $\Delta$  in the Tables) is still significant, as it can be seen in Tables 5, 6 and 7, but now they have less impact on the final error than the uncertainties in the decay constants  $f_D$  and  $f_{D^*}$  and in the charm quark mass. In these Tables we show in the first column the quantity which was varied, in the second the average coupling constant resulting from that variation, in the third the standard deviation and in the fourth the percentual significance of  $\sigma$ .

After scanning the space of reasonable values of all the parameters, we conclude that, in spite of the inherent uncertainties, the sum rules really point to a value of the coupling constant! Of course, as in most of QCDSR calculations, the lack of precision is due to the “usual suspects”, i.e., continuum threshold parameters, decay constants, heavy quark masses and condensates. A comparison of the Tables shows an intriguing aspect, namely that some of the input quantities affect each of the three sum rules in a quite different way. This may be a signal that some of the sum rules are less reliable than others. A deeper investigation of this question would involve several refinements, such as the calculation of  $\alpha_s$  corrections and higher order terms in the OPE.

Considering the results presented in the Tables, the couplings are:

$$g_{D^*D\rho}^{(D)} = 5.71 \pm 0.62 \text{ GeV}^{-1},$$

$$g_{D^*D\rho}^{(\rho)} = 5.87 \pm 0.53 \text{ GeV}^{-1},$$

and

$$g_{D^*D\rho}^{(D^*)} = 6.63 \pm 0.73 \text{ GeV}^{-1},$$



Quantity	$\langle g_{D^*D\rho}^{(D)} \rangle$	$\sigma$	$\sigma$ (%)
$\Delta$	5.95	0.87	14.7
$f_\rho$	5.76	0.01	0.1
$f_D$	5.30	0.64	12.0
$f_{D^*}$	5.80	0.40	6.8
$M^2$	5.76	0.05	0.8
$m_c$	5.70	0.30	5.6
$\langle \bar{q}q \rangle$	5.77	0.04	0.8

Table 6: Changes in  $g_{D^*D\rho}^{(D)}$  induced by changes in different quantities.

Quantity	$\langle g_{D^*D\rho}^{(D^*)} \rangle$	$\sigma$	$\sigma$ (%)
$\Delta$	7.00	1.00	14.3
$f_\rho$	6.61	0.07	1.1
$f_D$	6.11	0.74	12.0
$f_{D^*}$	6.69	0.46	6.8
$M^2$	6.65	0.19	2.8
$m_c$	6.61	0.06	0.8
$\langle \bar{q}q \rangle$	6.66	0.08	1.3

Table 7: Changes in  $g_{D^*D\rho}^{(D^*)}$  induced by changes in different quantities.

We can see that the three cases considered here, off-shell  $D$ ,  $\rho$  and  $D^*$ , give compatible results for the coupling constant. Considering all the uncertainties and taking the average between the obtained values we have:

$$g_{D^*D\rho} = (6.1 \pm 1.3) \text{ GeV}^{-1}, \quad (85)$$

Our results were obtained for certain concrete choices of currents, which represent charged states. Consequently, the obtained couplings are for charged states. As it will be discussed in the next section, from the coupling of charged states we can get the coupling of neutral  $\rho$  states, which will be identified with the “generic coupling”, through the relation:

$$g_{D^*D\rho} = g_{D^*D\rho^0} = \frac{g_{\rho^+ D^0 D^{*+}}}{\sqrt{2}} = \frac{g_{\rho^- D^0 D^{*-}}}{\sqrt{2}}. \quad (86)$$

Therefore the final value of the coupling constant listed in Table 4 is:

$$g_{D^*D\rho} = (6.1 \pm 1.3)/\sqrt{2} = (4.3 \pm 0.9) \text{ GeV}^{-1},$$

To close this section we emphasize that, from the analysis of the Tables we conclude that, in the present context, the average error of our calculations is in the range from 10 to 15 %.

## 6 Discussion

In this section we compare our results with other QCDSR calculations, in particular with light-cone QCD sum rules (LCSR) results, and also with results obtained with other techniques. Besides QCDSR, coupling constants can be estimated with the vector meson dominance (VMD) model, with heavy quark effective theory (HQET), with SU(4) symmetry relations, with effective models such as the constituent quark-meson model, with chiral models and with lattice QCD calculations (LQCD).

## 6.1 SU(4) and HQET

If SU(4) would be exact, several relations between the coupling constants should hold. Using the QCDSR results reported in Table 4 we can check to what extent these relations are satisfied. The relevant relations and their deviation from our results are shown in Table 8. They are ordered by increasing degree of violation. Remembering the typical uncertainties of 10 % to 15 % in our calculations, we can conclude that the first seven SU(4) relations are reasonably satisfied whereas the last six relations are badly violated. Although there is no rigorous systematics, we can clearly observe that violations occur mostly when there is a pion in the vertex.

SU(4) Relation	Violation
$g_{J/\psi DD} = g_{J/\psi D^* D^*}$	(7%)
$g_{\rho DD^*} = \frac{\sqrt{6}}{2} g_{J/\psi DD^*}$	(12%)
$g_{\rho DD} = \frac{\sqrt{6}}{4} g_{J/\psi DD}$	(17%)
$g_{\pi D^* D^*} = \frac{\sqrt{6}}{2} g_{J/\psi DD^*}$	(20%)
$g_{D^* D^* \rho} = \frac{\sqrt{6}}{4} g_{J/\psi D^* D^*}$	(20%)
$g_{DD\rho} = \frac{\sqrt{6}}{4} g_{J/\psi D^* D^*}$	(21%)
$g_{\rho D^* D^*} = \frac{\sqrt{6}}{4} g_{J/\psi DD}$	(25%)
$g_{\pi D^* D^*} = g_{\rho DD^*}$	(29%)
$g_{\rho DD} = g_{\rho D^* D^*}$	(36%)
$g_{D^* D\pi} = g_{D^* D^* \rho}$	(52%)
$g_{D^* D\pi} = \frac{\sqrt{6}}{4} g_{J/\psi D^* D^*}$	(62%)
$g_{D^* D\pi} = \frac{\sqrt{6}}{4} g_{J/\psi DD}$	(64%)
$g_{D^* D\pi} = g_{DD\rho}$	(70%)

Table 8: SU(4) relations between the coupling constants (on the left column) and their violation (in percentage on the right column) found in QCDSR.

We can also check the heavy quark spin symmetry relations [40], which are presented below with their deviation from our results (calculated with the values presented in Table 4 in parenthesis:

$$g_{\rho D^* D} = \frac{g_{\rho D^* D^*}}{m_{D^*}} \quad (45\%) \quad (87)$$

$$g_{J/\psi D^* D} = \frac{g_{J/\psi DD}}{m_D} \quad (22\%) \quad (88)$$

These relations come from HQET. Since charm is not heavy enough to ensure the validity of HQET, we would expect a significant violation of the above relations. In fact, considering the error in our calculations (88) is still satisfied whereas (87) is severely violated.

## 6.2 Light cone sum rules

In Table 9 we present a compilation of the estimates of the coupling constants  $g_{D^* D\pi}$  and  $g_{B^* B\pi}$  from distinct calculations. From this Table we see that our result in Ref. [19] is in a fair agreement with the LCSR calculation in Refs. [42, 44], but is still smaller than the experimental value [49]:  $g_{D^* D\pi} = 17.9 \pm 0.3 \pm 1.9$ . However, using a better way to extrapolate the QCDSR results based on a meson loop calculation, the result obtained in Ref. [37] is in an excellent agreement with the experimental value. From this Table we also see that LQCD results are in a very good agreement with the experimental value.

Approach	$g_{D^*D\pi}$	$g_{B^*B\pi}$
QCDSR [41]	$9 \pm 2$	$20 \pm 4$
QCDSR [41]	$7 \pm 2$	$15 \pm 4$
LCSR [42]	$11 \pm 2$	$28 \pm 6$
QCDSR [43]	$6.3 \pm 1.9$	$14 \pm 4$
LCSR [44]	$10.5 \pm 3$	$22 \pm 9$
QCDSR [19]	$14.0 \pm 1.5$	$42.5 \pm 2.6$
QCDSR plus meson loops [37]	$17.5 \pm 1.5$	$44.7 \pm 1.0$
LQCD [45]	$20 \pm 2$	
LQCD [46]	$18.8^{+2.5}_{-3.0}$	
dispersive quark model [47]	$18 \pm 3$	$32 \pm 5$
Dyson-Schwinger equations [48]	$15.8^{+2.1}_{-1.0}$	$30.0^{+3.2}_{-1.4}$

Table 9: Summary of estimates for  $g_{D^*D\pi}$  and  $g_{B^*B\pi}$ . These couplings refer to charged mesons  $\pi^\pm$ .

The basic difference between the QCDSR, described here, and the LCSR is the fact that, instead of considering the three-point function in Eq. (15), the central object in the LCSR is the correlation function of two meson currents between the vacuum and one on-shell meson state [50]:

$$\Gamma(q, p) = \int d^4x \ e^{iq \cdot x} \langle M_1(p) | T \{ j_3(x) j_2^\dagger(0) \} | 0 \rangle. \quad (89)$$

The idea is to expand the product of the currents near the light-cone  $x^2 = 0$ . This expansion is different from the local OPE expansion used in the QCDSR because it incorporates a summation of an infinite series of local operators [50]. In the case that  $M_1$  is the pion, the vacuum-pion matrix elements are expressed via pion light-cone distribution amplitudes (DA). Since the pion DA's have a well defined twist, the LCSR can be written in terms of a twist expansion. On the other hand, if  $M_1$  is not light, its DA does not have a well defined twist. If  $M_1$  is a heavy meson, like a  $B$  meson, the correlation function can be systematically expanded in the limit of large  $m_b$  in heavy quark effective theory [51]. However, for hadronic vertices involving only charmed mesons there is no well defined expansion for the correlation function in the LCSR approach. An attempt to use LCSR to calculate the  $D^*D^*\rho$  coupling constant was performed in [52]. The obtained value is quoted in Table 10. It is closer to SU(4) and to VMD (see below) than the value found in [23]. However, a discussion of some potential sources of uncertainties, such as the use of a relatively large value of the Borel mass and the possible continuum dominance, is still missing in [52].

### 6.3 Vector meson dominance

In the VMD model [2] a virtual photon with four-momentum  $q$  is emitted in the process  $eM \rightarrow eM$ , where  $M$  represents any meson. The photon can be decomposed into a sum of all neutral vector mesons including both isospin 0 and isospin 1. Then the vector meson couples with the external meson  $M$ . At  $q^2 = 0$  one can write:

$$\sum_{V=\rho,\omega,\phi,J/\psi,\dots} \frac{\gamma_V g_{VMM}}{m_V^2} = e, \quad (90)$$

where  $\gamma_V$  is the photon-vector-meson coupling that can be determined from the vector meson partial decay width to  $e^+e^-$ :

$$\Gamma_{V \rightarrow ee} = \frac{\alpha \gamma_V^2}{3m_V^3}. \quad (91)$$

Using the VMD model the couplings  $g_{\rho DD}$ ,  $g_{\rho D^*D^*}$ ,  $g_{J/\psi DD}$  and  $g_{J/\psi D^*D^*}$  were estimated in Ref.[32]. The couplings  $g_{\rho D^*D}$  and  $g_{J/\psi D^*D}$  were estimated in Ref. [33] by applying the VMD model to the

Coupling	QCDSR	VMD	Other models
$g_{\rho DD}$	$3.0 \pm 0.2$ [17]	$2.52$ [32]	
$g_{\rho D^* D}$ ( $\text{GeV}^{-1}$ )	$4.3 \pm 0.9$ [24]	$2.82$ [33]	$4.17 \pm 1.04$ [54]
$g_{\rho D^* D^*}$	$4.7 \pm 0.2$ [23]	$2.52$ [32]	$1.8 \pm 0.5$ [52]
$g_{\omega DD}$	$-2.9$ [53]	$-2.84$ [32]	
$g_{J/\psi DD}$	$5.8 \pm 0.9$ [22]	$7.64$ [32]	$8.0 \pm 0.5$ [40]
$g_{J/\psi D^* D}$ ( $\text{GeV}^{-1}$ )	$4.0 \pm 0.6$ [22]	$8.0 \pm 0.6$ [33]	$4.05 \pm 0.25$ [40]
$g_{J/\psi D^* D^*}$	$6.2 \pm 0.9$ [20]	$7.64$ [32]	$8.0 \pm 0.5$ [40]

Table 10: Summary of estimates for  $g_{VD^{(*)}D^{(*)}}$ . In the above couplings  $\rho$  stands for  $\rho_0$ .

radiative decay  $D^* \rightarrow D\gamma$ . The obtained values are presented in the Table 10 where we also present a summary of the predictions for the coupling constants in the  $VD^{(*)}D^{(*)}$  vertex.

In our approach the coupling constant is given by the value of the form factor at  $Q^2 = -m_M^2$ , where  $M$  is the off-shell vector meson. In the case of  $J/\psi$  this corresponds to  $Q^2 = -9.6 \text{ GeV}^2$  whereas for  $\rho_0$  the on-shell point is  $Q^2 = -0.6 \text{ GeV}^2$ . In the VMD model the vector meson has  $Q^2 = 0 \text{ GeV}^2$ . We would then expect our results to present a reasonable agreement with the VMD estimates of the  $\rho$  couplings and a significant disagreement with the VMD estimates of the  $J/\psi$  couplings. This pattern is not so evident in Table 10, which shows the approximate expected behavior in some cases but also shows discrepant behavior in other cases. All the form factors decrease as  $Q^2$  goes from the time-like to the space-like region and hence all the values shown in the left column of Table 10 will become smaller when calculated at  $Q^2 = 0 \text{ GeV}^2$ . This will improve the agreement with the VMD estimates in the case of the light vector mesons and will increase the disagreement with the heavy vector mesons. Since QCDSR are more reliable in the latter case, this comparison suggests that the use of VMD for heavy mesons is dangerous.

## 7 $J/\psi$ absorption and production

As an application of the form factors obtained above we address now the problem of  $J/\psi$  absorption and production in hadronic matter. With the Lagrangians (40) - (50) we are able to compute the process  $D\bar{D} \rightarrow J/\psi + \pi$ , which involves the diagrams in Fig. 20, the process  $D^*\bar{D} \rightarrow J/\psi + \pi$ , corresponding to the diagrams shown in Fig. 21 and also the process  $D^*\bar{D}^* \rightarrow J/\psi + \pi$ , corresponding to the diagrams in Fig. 22.

As extensively discussed in previous works, although the above Lagrangians and amplitudes are quite satisfactory from the point of view of symmetry requirements, their straightforward application to the computation of cross sections leads to unacceptably large results. This comes from the fact that the exchanged particles may be far off-shell and therefore they enter (or leave) a vertex with a very different resolving power. In one extreme case, a virtual  $J/\psi$  probing a  $D$  meson, may behave like a parton. Of course, when this happens, the compact  $J/\psi$  almost misses the large  $D$  and as a consequence the cross section of the whole process drops significantly. This physics of spatial extension and resolving power is contained in the form factors. It has been realized by many authors that calculations with and without form factors lead to results differing by up to two orders of magnitude! Therefore we simply *can not ignore the form factors*. We must include them in order to obtain reliable results!

Looking at the diagrams in Figs. 20, 21 and 22 we notice that we need the following form factors (and the corresponding coupling constants):  $g_{\pi DD^*}^{(D^*)}(t)$ ,  $g_{J/\psi DD}^{(D)}(t)$ ,  $g_{J/\psi DD^*}^{(D^*)}(t)$ ,  $g_{J/\psi DD^*}^{(D)}(t)$ ,  $g_{J/\psi D^* D^*}^{(D^*)}(t)$  and  $g_{\pi D^* D^*}^{(D^*)}(t)$ , where  $t$  is the usual momentum transfer squared and in the superscript in parenthesis we denote the off-shell particle. This is an important distinction, because the form factors in the same vertex, as we have seen, are very different when different particles are off-shell.

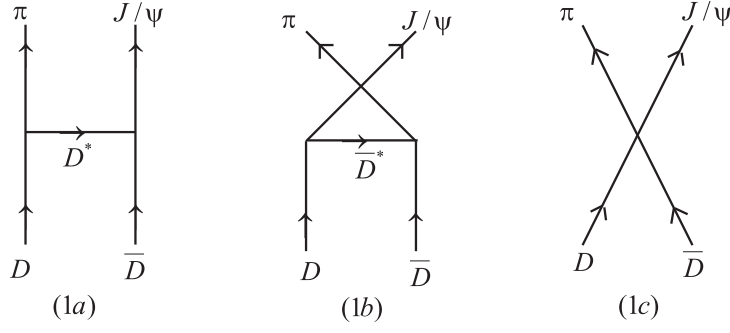


Figure 20: Diagrams which contribute to the process  $D\bar{D} \rightarrow J/\psi + \pi$ .

The cross sections for secondary  $J/\psi$  production is related to the annihilation through detailed balance. In Fig. 23 we show the  $J/\psi$  secondary production cross section as a function of  $\sqrt{s}$ , without form factors. In all Figures, the channels  $D\bar{D} \rightarrow J/\psi + \pi$ ,  $D\bar{D}^* \rightarrow J/\psi + \pi$  and  $D^*\bar{D}^* \rightarrow J/\psi + \pi$  are represented by solid, dashed and dotted lines respectively. In Fig. 24 we show the corresponding inverse reactions. As it can be seen, the cross sections have the same order of magnitude in both directions. Figs. 25 and 26 are the analogues of 23 and 24 when we include the form factors in the calculations. Of course, only these last two Figures correspond to realistic numbers. The comparison of the two sets of Figures is interesting to estimate the effect of form factors. In previous studies doing the same kind of comparison, as for example in [33], the introduction of form factors reduced the cross sections by factors ranging between 20 and 50 depending on the channel. In that work the form factor was the same for all vertices and the cut-off, not known, was estimated to be between 1 and 2 GeV. Our study is much more detailed and not only each vertex has its own form factor, but, depending on which particle is off-shell the form factor is different. The final effect of all these peculiarities is the reduction of the cross sections by a factor around 7. Although significant, this reduction is smaller than previously expected.

Fig. 25 contains our main results. The plotted cross sections can be compared with the results of [55] and, more directly, with [56]. In Fig. 2 of [55], although the variables in the plot are different, we can observe the same trend and relative importance of the three channels. In that work, the results were obtained with the quark model of [57]. Our curves share some features with the results of [56], such as, for example, the dominance of the  $DD^*$  channel and the falling trend of the  $DD^*$  and  $D^*D^*$  channels. The behavior of the  $DD$  channel is quite different. In the energy range of  $\sqrt{s} > 4.5$  GeV our cross sections are smaller by a factor of 2 ( $DD^*$ ) or 5 ( $D^*D^*$  and  $DD$ ). These discrepancies are large but they are expected since in [56] all channels include the final state  $J/\psi + \rho$ , which we did not include. In the model used by the Giessen group [56] the cross sections for  $D + \bar{D} \rightarrow J/\psi + \pi$  and  $D + \bar{D} \rightarrow J/\psi + \rho$  are similar and the same conclusion holds for the other initial state open charm mesons. If this would remain true in the effective Lagrangian approach, then our results including both final states would come closer to those of [56], giving thus a more theoretical support to the model considered there.

The exercise presented in this section was meant to illustrate the use of the charm form factors discussed in this review. The ultimate computation of charmonium interactions in a hot and dense medium should include other effects, not mentioned here. For recent works on the subject see, for example, [58, 59].

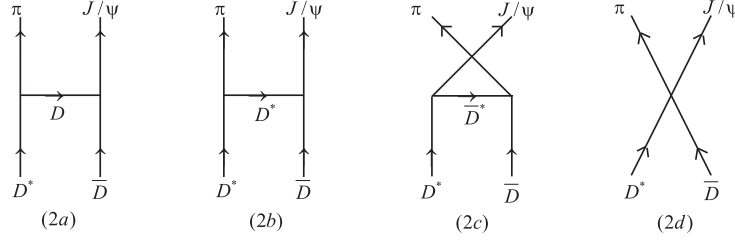


Figure 21: Diagrams which contribute to the process  $D^* \bar{D} \rightarrow J/\psi + \pi$ .

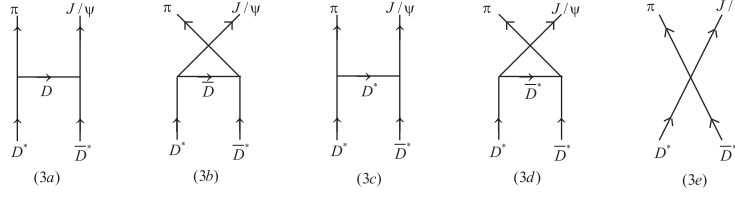


Figure 22: Diagrams which contribute to the process  $D^* \bar{D}^* \rightarrow J/\psi + \pi$ .

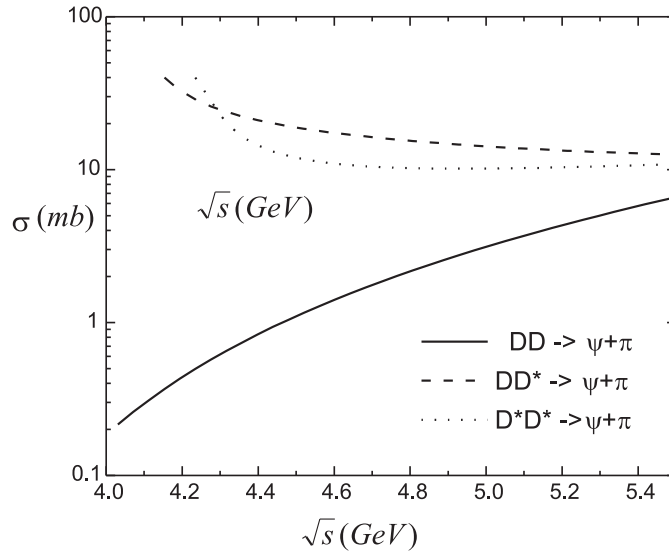


Figure 23:  $J/\psi$  secondary production cross section without form factors.

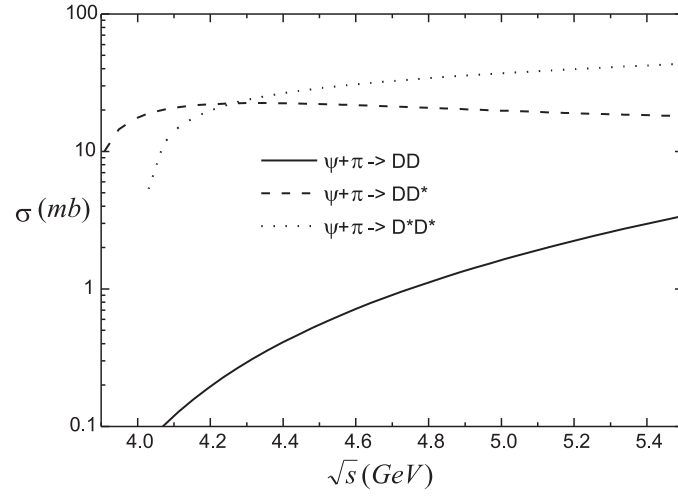


Figure 24:  $J/\psi$  absorption cross section obtained through detailed balance without form factors.

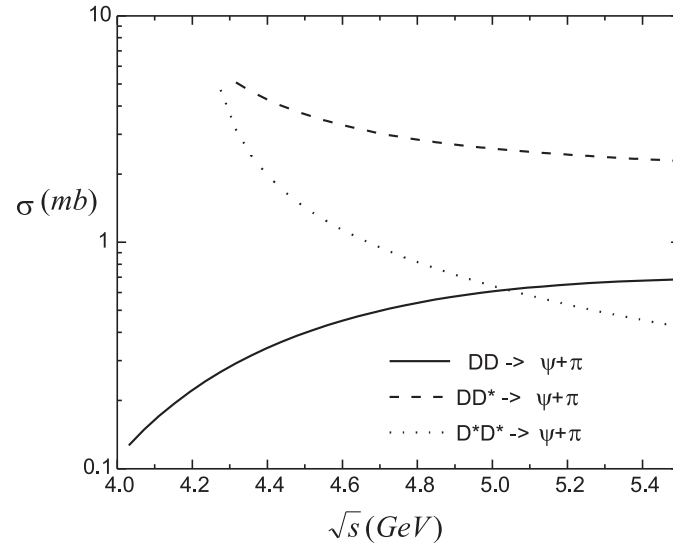


Figure 25:  $J/\psi$  secondary production cross section with form factors.

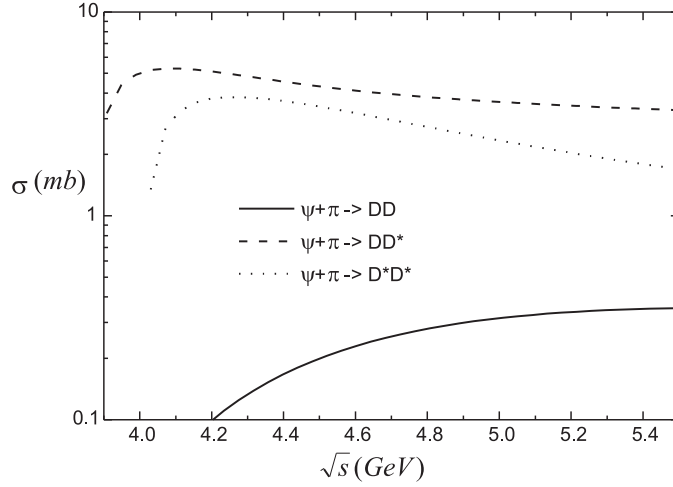


Figure 26:  $J/\psi$  absorption cross section obtained through detailed balance with form factors.

## 8 Summary

We have studied the form factors of vertices with charm mesons. They are relevant to understand data from heavy ion collisions at RHIC and LHC, from B decays at BELLE and BABAR and, in the future, charm production at PANDA. We have described how to calculate them with QCDSR and presented the results of our calculations. The comparison of the obtained coupling constants with those obtained with other methods shows that all the numbers have the same order of magnitude and the discrepancies between them go from a few percent to a factor two. In every approach there are improvements to be made and more accurate results are expected in the future. There are still vertices which have not been studied, such as those with  $\eta_c$ . With the already available charm form factors it is possible to address a number of problems of phenomenological interest. One of them, namely, the production and absorption of  $J/\psi$  in nuclear matter was discussed here and the huge effect of form factors was shown in detail. Moreover some of these form factors have been used in [13] to study resonances formed through meson exchange interactions.

Most of the calculations follow standard procedures in QCDSR but the extrapolation techniques to compute the coupling constant were developed by our group. We calculated two form factors for two off-shell mesons in the considered vertex. The simultaneous extrapolation of these form factors allowed the determination of the coupling constant. While this requirement proved to be crucial for finding the coupling, the inclusion of a third form factor, obtained by putting the third meson off the mass shell, with the subsequent triple extrapolation to obtain the coupling, did not bring any significant improvement in the results.

The extrapolation method used in our works has a systematic error which comes from the choice of the analytic form of the extrapolating functions. We considered only monopole, exponential and gaussian parametrizations. However there is no physical reason for choosing these forms. Using the  $D^*D\pi$  vertex for an exploratory study, we calculated the form factor computing the relevant hadronic loops. In this way there is no need to guess a particular form for the form factor. Since the hadronic loop calculation contains non-perturbative physics it should be reliable in low  $Q^2$  domain. The introduction of hadronic loops improved a lot our quantitative analysis of the  $D^*D\pi$  vertex. However we think that it would be premature to include it as an obligatory complement to the QCDSR formalism. Some loop diagrams were neglected because they were assumed to be less important but this must still be proven. Moreover the effective Lagrangian theories for other mesons and for baryons are less well known.

The disagreement between some of our results and the SU(4) predictions has still to be clarified.



The same is true for the estimates made with the help of light cone sum rules, heavy quark symmetry and vector meson dominance. From the perspective of QCDSR there is still room for improvements, as, for example, the inclusion of  $\alpha_s$  corrections and higher order condensates. An important extension of our program will be to systematically study vertices with charm and strange mesons. Some of them were already considered in Refs. [60, 61, 62, 63, 64].

Beyond individual technical improvements, we believe that the QCDSR community should make a joint effort dedicated to systematically compare results and methods and arrive at a consensus on the present status of the calculation of coupling constants. With this review we wish to take a step in this direction.

## Acknowledgments

This work has been partly supported by the brazilian funding agencies FAPESP and CNPq. We are deeply grateful to F. Carvalho, F.O. Durães, A. Lozea, R.D. Matheus, B. Osório Rodrigues, M.R. Robilotta, R. Rodrigues da Silva, C. Schat, S. Narison, Q. Zhao, E. Oset and E. Shuryak, for fruitful discussions.

## References

- [1] M.E. Peskin and D.V. Schroeder, *Introduction to quantum field theory*, Addison-Wesley Pub. Co., (1995); F.E. Close, *An introduction to quarks and partons*, Academic Press, (1979); F. Halzen and A. Martin, *Quarks and leptons: an introductory course on modern particle physics*, John Wiley, (1984).
- [2] Y. Nambu, Phys. Rev. 106 (1957) 1366; W.R. Frazer and J.R. Fulco, Phys. Rev. 117 (1960) 1609; J.J. Sakurai, Ann. Phys. 11 (1960) 1; M. Gell-Mann and F. Zachariasen, Phys. Rev. 124 (1961) 953; M. Gell-Mann, Phys. Rev. 125 (1962) 1067; T. H. Bauer *et al.*, Rev. Mod. Phys. 5 (1978) 261; [Erratum-ibid 5 (1979) 407.
- [3] S.G. Matinyan and B. Müller, Phys. Rev. C 58 (1998) 2994.
- [4] T. Matsui and H. Satz, Phys. Lett. B 178 (1986) 416.
- [5] K. L. Haglin and C. Gale, Phys. Rev. C 63 (2001) 065201;
- [6] F.O. Durães, H. c. Kim, S.H. Lee, F.S. Navarra and M. Nielsen, Phys. Rev. C 68 (2003) 035208; F. O. Durães, S. H. Lee, F. S. Navarra and M. Nielsen, Phys. Lett. B 564 (2003) 97.
- [7] F. K. Guo, C. Hanhart, G. Li, U. G. Meissner and Q. Zhao, Phys. Rev. D 83 (2011) 034013.
- [8] <http://www.gsi.de/fair>
- [9] M. Nielsen, F.S. Navarra, S.H. Lee, Phys. Rept. 497 (2010) 41.
- [10] N. Brambilla *et al.*, Eur. Phys. J. C 71 (2011) 1534.
- [11] N. Isgur, K. Maltman, I. Weinstein and T. Barnes, Phys. Rev. Lett. 64 (1990) 161; H. Lipkin, Nucl. Phys. B 244 (1984) 147; H. Lipkin, Phys. Lett. B 179 (1986) 278; H. Lipkin, Nucl. Phys. B 291 (1987) 720; H. Lipkin and B.S. Zou, Phys. Rev. D 53 (1996) 6693; P. Geiger and N. Isgur, Phys. Rev. Lett. 67 (1991) 1066; V.V. Anisovich, D.V. Bugg, A.V. Sarantsev and B.S. Zou, Phys. Rev. D 51 (1995) R4619; X.Q. Li, D.V. Bugg and B.S. Zou, Phys. Rev. D 55 (1997) 1421.

- [12] X. Liu, B. Zhang and S. L. Zhu, Phys. Lett. B 645 (2007) 185.
- [13] R. Molina, T. Branz and E. Oset, Phys. Rev. D 82 (2010) 014010.
- [14] R. Molina and E. Oset, Phys. Rev. D 80 (2009) 114013.
- [15] R. Molina, H. Nagahiro, A. Hosaka and E. Oset, Phys. Rev. D 80 (2009) 014025.
- [16] F.S. Navarra, M. Nielsen, M.E. Bracco, M. Chiapparini, C.L. Schat, Phys. Lett. B 489 (2000) 319.
- [17] M.E. Bracco, M. Chiapparini, A. Lozea, F.S. Navarra, M. Nielsen, Phys. Lett. B 521 (2001) 1.
- [18] R.D. Matheus, F.S. Navarra, M. Nielsen, R. Rodrigues da Silva, Phys. Lett. B 541 (2002) 265.
- [19] F.S. Navarra, M. Nielsen, M.E. Bracco, Phys. Rev. D 65 (2002) 037502.
- [20] M.E. Bracco, M. Chiapparini, F.S. Navarra, M. Nielsen, Phys. Lett. B 605 (2005) 326.
- [21] F. Carvalho, F.O. Durães, F.S. Navarra, M. Nielsen, Phys. Rev. C 72 (2005) 024902.
- [22] R.D. Matheus, F.S. Navarra, M. Nielsen, R. Rodrigues da Silva, Int. J. Mod. Phys. E 14 (2005) 555.
- [23] M.E. Bracco, M. Chiapparini, F.S. Navarra, M. Nielsen, Phys. Lett. B 659 (2008) 559.
- [24] B. Osório Rodrigues, M.E. Bracco, M. Nielsen, F.S. Navarra, Nucl. Phys. A 852 (2011) 127.
- [25] M.A. Shifman, A.I. Vainshtein and V.I. Zakharov, Nucl. Phys. B 147 (1979) 385.
- [26] L.J. Reinders, H. Rubinstein and S. Yazaki, Phys. Rept. 127 (1985) 1.
- [27] For a review and references to original works, see e.g., S. Narison, “QCD as a theory of hadrons”, Camb. Monogr. Part. Phys. Nucl. Phys. Cosmol. 17 (2002) 1; “QCD spectral sum rules”, World Sci. Lect. Notes Phys. 26 (1989) 1; Phys. Rept. 84 (1982) 263.
- [28] B.L. Ioffe, Nucl. Phys. B 188 (1981) 317.
- [29] R.D. Matheus, F.S. Navarra, M. Nielsen and R. Rodrigues da Silva, Phys. Rev. D 76 (2007) 056005.
- [30] B. Ioffe and A. Smilga, Nucl. Phys. B 232 (1984) 109.
- [31] E. de Rafael, “An introduction to sum rules in QCD”, arXiv:hep-ph/9802448.
- [32] Z. Lin and C.M. Ko, Phys. Rev. C 62 (2000) 094903.
- [33] Y. Oh, T. Song and S.H. Lee, Phys. Rev C 63 (2001) 034901.
- [34] Particle Data Group, K. Hagiwara et al., Phys. Rev. D 66 (2002) 1.
- [35] B. Osório Rodrigues, M.E. Bracco and M. Chiapparini, AIP Conf. Proc. 1296 (2010) 302.
- [36] R. Rodrigues da Silva, R.D. Matheus, F.S. Navarra, M. Nielsen, Braz. J. Phys. 34 (2004) 236.
- [37] F.O. Durães, F.S. Navarra, M. Nielsen and M.R. Robilotta, Braz. J. Phys. 36 (2006) 1232.
- [38] A. Szczurek, H. Holtmann and J. Speth, Nucl. Phys. A 605 (1996) 496.
- [39] D.B. Leinweber, Annals Phys. 254 (1997) 328.

- [40] A. Deandrea, G. Nardulli and A.D. Polosa, Phys. Rev. D 68 (2003) 034002.
- [41] P. Colangelo *et al.*, Phys. Lett. B 339 (1994) 151.
- [42] V.M. Belyaev *et al.*, Phys. Rev. D 51 (1995) 6177.
- [43] H.G. Dosch and S. Narison, Phys. Lett. B 368 (1996) 163.
- [44] A. Khodjamirian *et al.*, Phys. Lett. B 457 (1999) 25.
- [45] D. Bećirević and B. Haas, arXiv:0903.2407 [hep-lat].
- [46] A. Abada *et al.*, Phys. Rev. D 66 (2002) 074504.
- [47] D. Melikhov, Eur. Phys. J. C 4 (2002) 2.
- [48] B. El-Bennich, M.A. Ivanov and C.D. Roberts, Phys. Rev. C 83 (2011) 025205.
- [49] A. Anastassov *et al.*, (CLEO Collaboration), Phys. Rev. D 65 (2002) 032003.
- [50] P. Colangelo and A. Khodjamirian, hep-ph/0010175.
- [51] A. Khodjamirian, T. Mannel and N. Offen, Phys. Rev. D 75 (2007) 054013.
- [52] Z. G. Wang and Z. B. Wang, Chin. Phys. Lett. 25 (2008) 444.
- [53] L.B. Holanda, R.S. Marques de Carvalho and A. Mihara, Phys. Lett. B 644 (2007) 232.
- [54] Z. H. Li, T. Huang, J. Z. Sun and Z. H. Dai, Phys. Rev. D 65 (2002) 076005.
- [55] C.M. Ko, B. Zhang, X.N. Wang, X.F. Zhang, Phys. Lett. B 444 (1998) 237.
- [56] E.L. Bratkovskaya, W. Cassing and H. Stöcker, Phys. Rev. C 67 (2003) 054905; W. Cassing, K. Gallmeister, E.L. Bratkovskaya, C. Greiner and H. Stöcker, Prog. Part. Nucl. Phys. 53 (2004) 211.
- [57] K. Martins, D. Blaschke and E. Quack, Phys. Rev. C 51 (1995) 2723.
- [58] A. Bourque and C. Gale, Phys. Rev. C 80 (2009) 015204.
- [59] R. Rapp, D. Blaschke and P. Crochet, Prog. Part. Nucl. Phys. 65 (2010) 209.
- [60] M.E. Bracco, A.J. Cerqueira, M. Chiapparini, A. Lozea and M. Nielsen, Phys. Lett. B 641 (2006) 286.
- [61] K. Azizi and H. Sundu, J. Phys. G 38 (2011) 045005.
- [62] H. Sundu, J.Y. Sungu, S. Sahin, N. Yinelek and K. Azizi, arXiv:1103.0943 [hep-ph].
- [63] Z.G. Wang, Nucl. Phys. A 796 (2007) 61; Eur. Phys. J. C 52 (2007) 553.
- [64] Z.G. Wang, S.L. Wan, Phys. Rev. D 74 (2006) 014017.

